Copyright Undertaking

RARE EARTH-DOPED PEROVSKITE-STRUCTURED OXIDES WITH STRONG ELASTICO-MECHANOLUMINESCENCE

LI YIN

MPhil

The Hong Kong Polytechnic University

2021

The Hong Kong Polytechnic University

Department of Applied Physics

Rare Earth-doped Perovskite-structured Oxides with Strong Elastico-mechanoluminescence

Li Yin

A thesis submitted in partial fulfilment of the requirements
for the degree of Master of Philosophy

August 2020

CERFITICATE OF ORIGINALITY

I hereby declare that this thesis is my own work and that, to the best of my knowledge and belief, it reproduces no material previously published or written, nor material that has been accepted for the award of any other degree or diploma, except where due acknowledgement has been made in the text.

____________________________ (Signed)

Li Yin (Name of student)

Abstract

Mechanoluminescence (ML), which refers to the luminescence triggered by an external mechanical load, has been investigated by many scholars since 19th century. The application of ML materials was limited until the research of non-destructive ML induced by elastic deformation was started. Different types of materials have been found exhibiting ML response. However, only a few of them can be practically used in applications. ML materials are generally used as stress sensors in applications and some of them are for dynamic pressure mapping. The working principle of ML, which is related to the release of trapped charge carriers, is still unsolved. Many models have been proposed to explain the observations for specific type of ML materials, but the availability of those theories to other ML materials is still controversial. This is the most significant obstacle for the ML research for the research of new ML materials and new applications. To date, most of the well-developed ML materials can yield greenish-blue ($ZnS: Cu^+$, $SrAl_2O_4: Eu^{2+}$) to yellow ($ZnS: Mn^{2+}$) emissions under applied stress. Therefore, for developing a complete display system, ML materials with the capability of emitting red light are highly desirable.

In this work, we report the development of a new ML material, i. e., $Ba_{0.15}Ca_{0.85}Ti_{0.9}Zr_{0.1}O_3: 0.2Pr^{3+}$ (abbreviated as CBTZ-Pr) that possesses a perovskite structure and exhibits strong red emissions under applied stress. Like the other typical ML emissions, the red emission decays with each application of mechanical load. However, it can be recovered after a short-period irradiation with UV light since the elastic deformation would not remain any permanent destruction to the material and is thus called elastic-mechanoluminescence (EML). In this work, the EML responses of CBTZ-Pr is investigated via the application of a tensile stress and the light emission

phenomenon is photographed and its intensity is measured. The strong red emission, with its intensity peaked at 611nm, can easily observed by naked eye and captured by photos. The perovskite-structure CBTZ-Pr oxide shows a naturally originated diphase structure, containing two regions or phases of different chemical compositions separated by a clear boundary. The thermoluminescence behavior of the oxide is also examined for investigating the charge trapping centers, in particular their relative depth in the energy band structure. Based on those results, an electron-tunneling model is proposed to elucidate the mechanism of the observed EML phenomenon. Our findings in this work, in particular the proposed mechanism, provide essential information and knowledge for the further development of a new ML material system based on perovskite-structure $Ba_xCa_{1-x}Ti_yZr_{1-y}O_3$ oxides.

Acknowledgements

I would like to express my best appreciation to my chief supervisor, Prof. K. W. Kwok. During the years of research work, he provides me the best support both in study and student life. His help gives me confidence in research study and future research life. With his valuable advice and patient guidance on my research work, I can fluently finish the study as research student.

I would also like to express my gratitude to Prof. J. H. Hao for providing appropriate measuring environment of the ML tests. I would like to thank the technical support by Materials Research Centre of the Hong Kong Polytechnic University. Only with their help I can smoothly conduct my experiment work.

I also want to appreciate the assistantship provided by all the members in Prof. Kwok's group for their help both in technique and study life. Specially, I would like to give my best gratitude to my colleague, Dr. Man Chung Wong for his generous help in both the experiment and theory study. Besides, a warm thank is given to Mr. Zhengnan Zhang, for his assistantship in experiment.

Finally, I would like to sincerely thank my parent and friends for their support to my research study life. It is their support help me overcome all the difficulties met during the two years of research life.

List of content

List of Figure and Table

List of acronyms

ML	Mechanoluminescence
LEDs	Light-emitting diodes
FML	Fracto-Mechanoluminescence
PML	Plastico-Mechanoluminescence
EML	Elastico-Mechanoluminescence
CBTZ-Pr	$Ba_{0.15}Ca_{0.85}Ti_{0.9}Zr_{0.1}O_3$: Pr^{3+}
BCTZ-Pr	$Ba_{0.85}Ca_{0.15}Ti_{0.9}Zr_{0.1}O_3$: Pr^{3+}
EL	Electroluminescence
TL	Thermoluminescence
PL	Photoluminescence
PVA	Polyvinyl Alcohol
XRD	X-Ray Diffraction
PDMS	Polydimethylsiloxane
BSE	Back-Scattered Electron
SEM	Scanning Electron Microscope
EDS	Energy Dispersive x-ray Spectroscopy

UV	Ultra-Violet
PMT	Photon counting Meter
CTS	Charge Transfer State
EPR	Electron Paramagnetic Resonance

Chapter 1 Introduction

1.1 Mechanoluminescence

1.1.1 Luminescence

Luminescence refers to the cold-light emission after the excitation through different ways, such as photon absorption, heat absorption, and electric field stimulation. Different from incandescent lamps, there is no heat produced during the process of luminescence. Therefore, unlike blackbody radiation, the photons emitted by way of luminescence are generally caused by the transition of electrons to lower energy levels in atoms. The occurrence of luminescence can be basically separated into three steps: energy absorption, energy transfer and light emission. A luminescent material generally consists of a host lattice, activators (optional) and luminescence centers. The energy will be firstly absorbed by the host lattice, which can be organic or inorganic crystals or crystalline materials, or the activators, and then transmitted to the luminescence centers for inducing the light emission. Among the three steps, energy transfer attracts the most attention from scientists, since it can occur at different ways depending on the compositions of the materials. In order to better understand the mechanism of mechanoluminescence, an introduction of different energy transfer ways in luminescence will be given. In fact, according to the way of energy transfer, the luminescent materials can be classified into two types: intrinsic luminescent materials and extrinsic luminescent materials.

1.1.1.1 Intrinsic luminescence

In intrinsic luminescent materials, the transfer of energy is realized through band-to-band luminescence, exciton-luminescence, or cross-luminescence. Band-to-band luminescence is caused by the radiative recombination of an electron in the conduction band and with a hole in the valence band, which have enough energy to move freely inside the crystal. It generally occurs in semi-conductors, like silicon and some IIIb-Vb compounds. It is the fundamental mechanism of the intensive light emission observed in light-emitting diodes (LEDs) and semiconductor lasers.

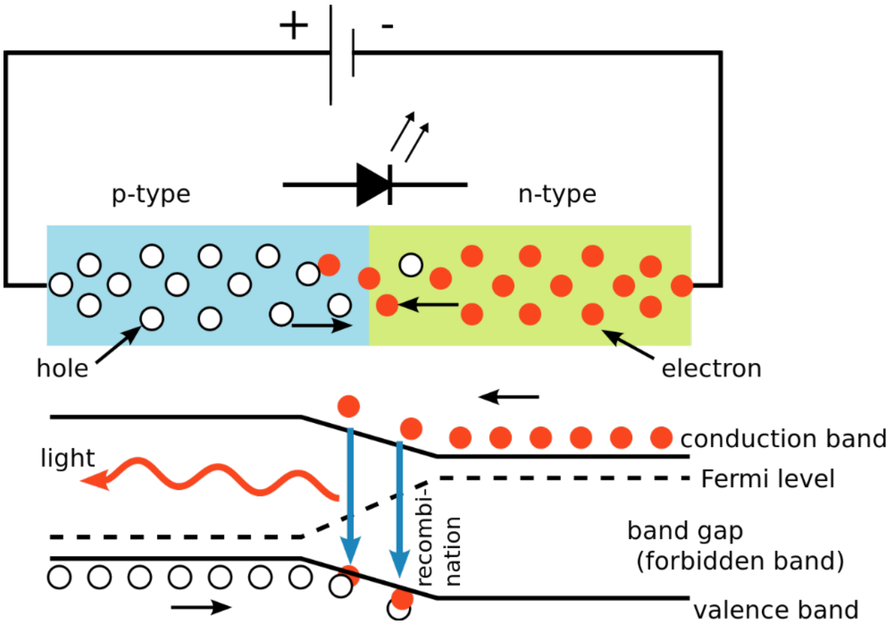

Figure 1.1 Band-to-band luminescence in LEDs[1]

The band-to-band luminescence tends to occur at high temperature. At lower temperatures, the excitons will be generated instead of directly emitting light when recombination happens. Excitons are formed as excited positive and negative charge carriers are interacting with each other and bound together by electrostatic force. An exciton has no charge since the charge is neutralized during the interaction. Therefore, it can move in a crystal and transfers its energy for inducing light-emission. Excitons can be divided into two types: the Wannier exciton and the Frenekel exciton. A Wannier exciton is formed when an electron in the conduction band interacts with a hole in the valence band. They are bound together due to the attraction of electrostatic force and no net charge is presented. When the electric potential energy originated from the attraction is larger than the thermal energy, the Wannier exciton is relatively stable. The exciton-luminescence of it is realized through the recombination of charge carriers of the exciton. The difference between Wannier exciton and Frenkel exciton is the expansion of carriers' wave function, which correspond to the space where the movement of charge carriers of the exciton cover. This difference is originated from the difference in the bound strength between the electron and hole. In a Frenkel exciton, the bound is strong enough so that the expansion is smaller than the lattice constant while the condition is opposite for the Wannier exciton. Therefore, the Frenekel exciton are more commonly formed in organic molecular crystals and inorganic composite with transition-metal ions inside.

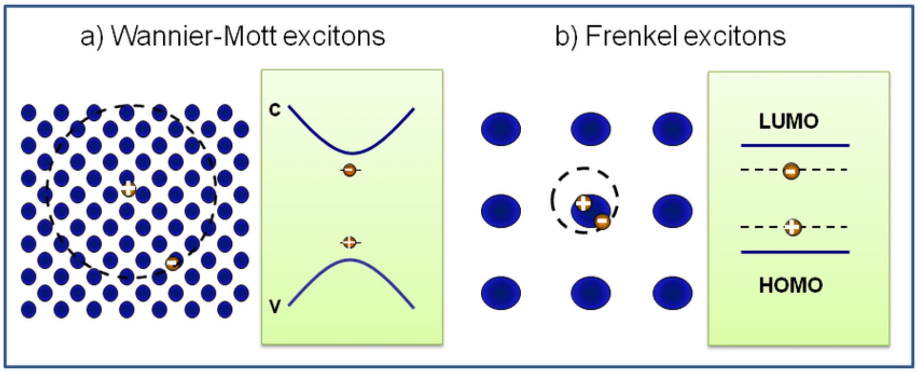

Figure 1.2 Comparation of Wannier exciton (Wannier-Mott exciton) and Frenkel exciton.[2]

Cross-luminescence occurs when the electrons in the valence band recombine with holes in the outer most core band, and the band gap energy is larger than the energy difference between the outer most core band and the top of valence band. It has been commonly observed in alkali halides, alkaline-earth halides, and double halides [3].

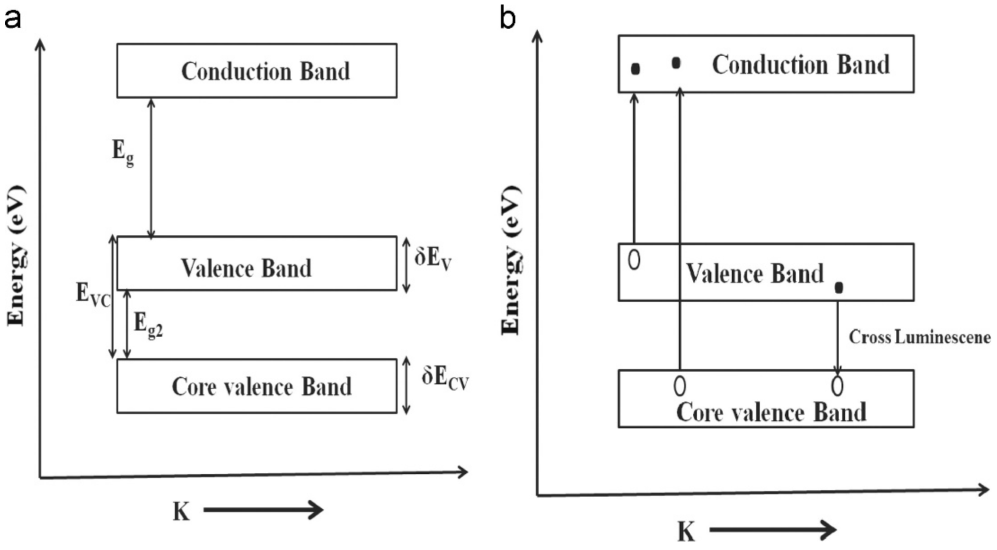

Figure 1.3 Schematic band energy diagram shows (a) the energy distribution and (b) the process of cross-luminescence[4]

1.1.1.2 Extrinsic luminescence

The energy transfer process in extrinsic luminescence materials is different from that in intrinsic luminescence materials because of the existence of luminescence center, which is generally formed by doped impurities. In fact, most phosphors have been used in practical applications are belongs to this category. The extrinsic luminescence can be classified into two types: unlocalized and localized luminescence, depending on the different ways of energy transfer.

For unlocalized luminescence, Free electrons in the conduction band and holes in the valence band of the host lattice atoms are involved in the forming donor-acceptor pairs or the isoelectronic traps. The donor-acceptor pairs are generally formed in semiconductors that simultaneously doped by both donors and acceptors. These donor and acceptor impurities will compensate each other at normal condition. Under irradiation at relatively low temperature, electrons could be trapped into donor impurities and form neutral donors while holes also be trapped to form neutral acceptors. Some of those neutral donors will then combine with neighboring neutral acceptors and form donor-acceptor excitons for inducing luminescence. As shown in Figure 1.4, a donor-acceptor pair consisting of a neutral donor and neutral acceptor will become charged with the radiative decay of the exciton.

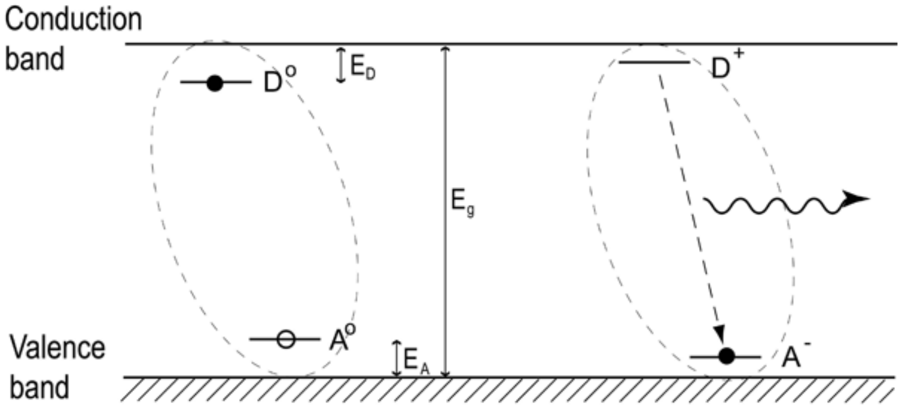

Figure 1.4 Donor-acceptor pair induced luminescence[5]

An isoelectronic trap is formed by a substitutional atom with the same amount of valence electrons as the original atom. The different electronic core structure of the substitutional atom will induce highly localized impurity states, called isoelectronic traps, in the band gap [6]. The isoelectronic traps can significantly change the optical properties of the host lattice, specifically, improving the efficiency of radiative recombination. For this reason, isoelectronic traps have been widely utilized in electroluminescence devices[7, 8].

For localized extrinsic luminescence, the energy absorption, energy transfer and light emission are restricted in the localized domain of luminescence center. It can be furtherly classified into two kinds, e.g. allowed transitions between s-p energy bands, s^2-sp bands and f-d bands, and forbidden transition, e.g. d-d (transfer inside the same electron orbital) transitions and f-f transitions [9].

1.1.2 Definition of Mechanoluminescence

Mechanoluminescence (abbreviated as ML) is a kind of luminescence as a reaction to mechanical excitation. It involves a transfer from mechanical energy to radiant energy. Before the general use of "Mechanoluminescence", "Triboluminescence" has also been broadly used in many academic publications in 19th century. It was created in 1888 by Wiedemann using Greek word "triben", which has a meaning of "rub" in Greek [10]. This phenomenon was firstly discovered by coincidence when a flash of light is observed during the smashing of loafsugar. This record can be found in Francis Bacon's book in 1605 [11]. ML, which was called "Triboluminescence" at that time, is regarded as one of the most ancient forms of luminescence since its occurrence does not need any artificial preparation.

Instead of being a synonym as Mechanoluminescence as at previous time, nowadays, "Triboluminescence" refers to emission of light when two different materials get contacted or separated with each other in some academic papers [12]. It may be caused by different reasons, such as the piezoelectric field or chemical reaction generated when they get contacted or separated. Although "Triboluminescence" is still widely used nowadays, it may be more accurate to use ML to summarize all kinds of mechanical-load-caused luminescence. Since "tribo" cannot include all kinds of mechanical stimuli, such as scratching, tensile load, torsion and vibration [13]. Apart from those different forms of forces, ML can also be triggered by thermal shocks, i.e., a dramatic change in the temperature of the material. In addition, ML can also be induced by the internal change of crystal structure, such as the growth of crystal material and transition of crystal phase [14].

Since ML can be excited by various type of external stimuli, it is necessary to classify them for convenience of discussion. The classification of ML also varies in different journal papers, in order to emphasize the corresponding property in their research. Among those different schemes, the classification by the kind of deformation is the most frequently used in current research.

1.1.3 Classification of Mechanoluminescence

When a mechanical stimulus is applied to a material, deformation of the material will occur. Depending on the stress level, the material will have different types of deformation. If the stress is low and the strain of the material can return to zero when the stress is released, the type of deformation is called “elastic deformation”. With the increase of the stress, the material cannot restore its origin dimensions. At this stage, “plastic deformation” is used to describe the extent of deformation. When the stress is strong enough, the material will break, and the deformation is called “fracture”. It is also irreversible, as the material’s structure has undergone a destructive damage in certain regions. According to the extent of deformation, ML can be categorized into three types: Fracto-Mechanoluminescence (FML), Plastico-Mechanoluminescence (PML) and Elastico-Mechanoluminescence (EML).

FML is the most common one among those three kinds of ML. In fact, approximately 50% of inorganic salts and organic solids exhibit FML when they experience a fracture [9]. Therefore, it is the first discovered type of ML. It can be triggered by different stimuli. The light emission may be due to the breakage of chemical bonds, which will release a considerate amount of energy and charge ambient gas or doped luminescent centers. In addition, as a result from the fracture, crack may propagate inside the material and new surfaces will be formed. The temperature and pressure at the tip of crack propagation will be high so that the luminescence will possibly be triggered by thermal energy at the tip. In addition to the thermal energy, electrical potential may be produced because of the movement of charged dislocation caused by the mechanical load or the potential difference between charged fracture planes and grinding tool. Apart from the electric potential, the external environment should also be considered, especially the surrounding gases, which may emit lighting through the gas discharge. Some materials can even absorb the photons emitted by gas discharge and subsequently induce photoluminescence, which is called tribophotoluminescence (TPL) and recorded in many researches[15, 16]. Therefore, the explanation of an FML process may be relatively complex since a single sparkling of light may involve many different physical or chemical reactions. It is meaningful to explore the details of each reaction occurred during an FML process for a better understanding of the mechanism. As for the development of application, the practice usage of this property is hardly worked out due to the irreversible damage to materials caused by FML. Although some of them can emit such intense light that can be sensed by naked eyes [17-19], they have seldom been utilized in practical applications because of the irreversible damages. Instead, they have been applied in fracture sensing systems like damage monitoring [20].

Similar to FML, PML also results in unrecoverable deformations. Although the material does not break, the PML will not repeat, unless new plastic deformation occurs [21]. Therefore, it is also difficult to be utilized in practical applications. As a result, the researches about EML has attracted more attention from scholars since the first discovery of EML materials such as $SrAl_2O_4$: Eu^+, Dy^+ and ZnS: Mn^{2+} in late 1990s [14, 22]. The intense emissions and recoverable characteristic make EML become strong candidates for sensing applications. After that, research about the improvement in emission intensity and development of new EML materials have been constantly conducted. More and more EML materials are discovered to fulfill the requirement of specific application. Although only EML materials can be put into practical use, the research of FML and PML materials are also necessary for better understanding of ML emission. Therefore, different ML materials will be introduced in the next paragraph, not only restricted to EML materials with practical application, to provide a clear view of research progress in the field.

1.1.4 Mechanoluminescence Materials

Research about ML materials can be mainly divided into two periods: before and after the invention of the photomultipliers. Before 1950s, the discovery of ML materials was based on visually observation, i.e., by the naked eyes of researchers' eyes in dark adapted environment. According to a rough estimation, approximately 400-500 ML materials, including organic and inorganic ones were discovered by_visual observation [10]. The number of ML materials is numerous since the ML emission can be induced by various mechanisms, especially FML emissions. Since 50% of inorganic materials exhibit ML, as stated in Chapter 1.1.3, it is not meaningful to list all of them. In this section, some important ML materials which have significant impact on the whole research progress or have a large potential for applications will be introduced.

1.1.4.1 X-ray or γ-ray irradiated Akali Halide

X-ray or γ-ray irradiated Alkali Halide is a common type of ML material, which has a long history since its discovery in 1930s. Generally, normal alkali halide without irradiation will emit FML, i.e., emitting light at fracture. After irradiation of X-ray or γ-ray or metal-vapor treatment, color centers are created in the materials, some of them will emit EML and PML. In fact, the performance of X-ray or γ-ray irradiated alkali halide is relative satisfying at the first application of mechanical load. For those emitting EML, the light intensity is linearly proportional to the applied stress [23]. On the other hand, the light intensity for PML will be proportional to the mechanical power. As it will not emit light again unless a new plastic deformation occurs, it is also called memory effect [21]. However, the application of alkali halide is limited by its weak emission intensity and unrepeatable EML emissions (i.e., the EML emission cannot be repeated although the mechanical deformation is elastic and recoverable).

1.1.4.2 Wurtzite ZnS

ZnS is a binary material which is much more popular than colored alkali halide. The study conducted in 1990s reports an intense yellow EML emission of $ZnS:Mn^{2+}$ [22]. The emission is intense enough to be observed by human eyes. Hence, they have proposed to utilize $ZnS: Mn^{2+}$ as artificial skin for detecting mechanical load. Another research conducted in 2010s combines the ZnS with Cu dopant [24]. By embedding the $ZnS: Cu^{+}$ particles in polydimethylsiloxane, they have fabricated composite films which can emit bright greenish-blue ML emission. The ML process can be repeated for approximately 100000 times and exhibits self-recovery property. The excellent performance makes the composite film a strong candidate for numerous ML applications. Apart from these two typical researches, many attempts have been conducted to further improve the performance, such as changing the dopants, co-dopants and co-operating with piezoelectric materials.

As one of the most reliable ML materials, many researches about ML material applications is based on wurtzite ZnS. They generally work as a mechanical load sensor to give an invigilation on the internal stress distribution. Specially, ZnS:Mn^{2+} can even realize dynamic pressure mapping and be used to record the signing habit of users [25].

1.1.4.3 Wurtzite CaZnOS

Based on the packing of tetrahedra layers, CaZnOS can also be classified as a wurtzite-liked material. CaZnOS exhibits ML response after doping with Cu^{+}, Mn^{2+} and other rare-earth elements. However, it cannot self-recover after repeated cycles like ZnS[26]. Among various dopants, only the doping of Cu^{+} can make CaZnOS show persistent luminescence (similar to ZnS). It indicates that traps corresponding to ML is different from persistent luminescence in some cases.

1.1.4.4 (Sr, Ca, Ba) Al_2O_4: RE (Tridymite)

$SrAl_2O_4$: Eu^{2+} was discovered to be non-destructive EML in 1990s, which ignites the research passionate in ML field. Together with ZnS: Mn^{2+}, they showed a big potential for stress detecting applications while causing no destructive damage of the material. Different from self-recovered ZnS: Mn^{2+}, $SrAl_2O_4$: Eu^{2+} needs UV exposure to recover for exhibiting repeatable EML. The emission of photons having a wavelength of 520nm is arisen from the transition between energy levels of $4f^7$ and $4f^65d^1$ of Eu. Apart from this, the ML spectrum of $SrAl_2O_4$: Eu^{2+} has the same peak position as the PL spectrum, proving the luminescence-center role of Eu.

$CaAl_2O_4$: (Eu^{2+}, Tb^{3+}), (Sr, Ba) Al_2O_4: (Dy^{3+}, Eu^{2+}/Eu^{3+}), (Sr, Ca) Al_2O_4: Dy^{3+} and Zn_2 (Ge, Si) O_4: Mn^{3+} have similar tridymite-like structure to $SrAl_2O_4$: Eu^{2+}. These ML materials can also show afterglow after exposure of UV light. Therefore, they are also called phosphor-type ML materials when explaining the mechanism of ML.

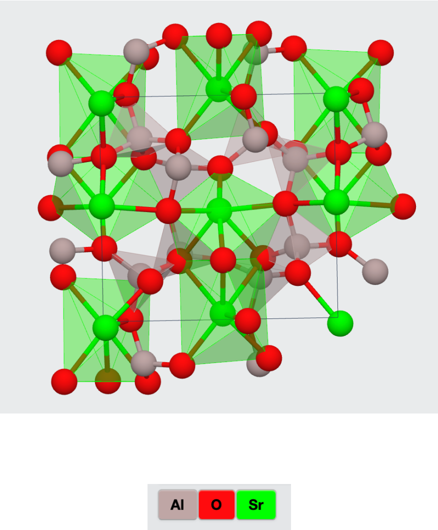

Figure 1.5 Structure of $SrAl_2O_4$ [27]

(Ba, Ca)(Ti, Zr)O_3: Pr, which is the material explored in this thesis is not included in the above classifications. Similar to some ML materials, it consists of a host, (Ba, Ca)(Ti, Zr)O_3 and a dopant, Pr^{3+}. To better understand the working principle of ML which contains the interaction between the host and dopant, they are introduced separately in following sessions.

1.2 Perovskite

(Ba, Ca)(Ti, Zr)O_3, the host lattice, belongs to a popular material group in both optical and electronic field: perovskite. Perovskite refers to the crystalline materials have a similar structure to $CaTiO_3$. The general unit formula of perovskite is ABX_3, where A and B are cations and X is an anion. Cations at the size of A-site is usually larger than the B-site cations. A conventional perovskite is with a face-centered cubic structure is shown in Figure 1.6.

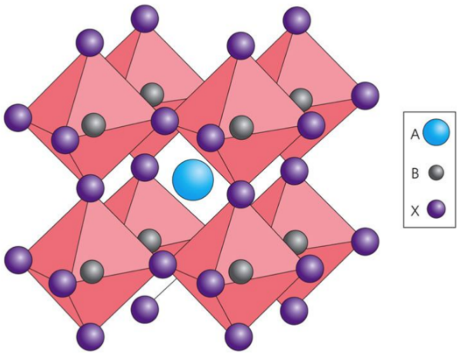

Figure 1.6 General structure of perovskite [28]

In a unit cell, the A-site cation is at the corner of the cube, the B cations sit at the body-center position while the X anions occupy the face-centered positions.

1.2.1 Halide perovskite

Based on the type of the X anions, perovskite can be classified as halide and oxide. For photovoltaic studies, a large number of researches have been conducted on halide perovskites. A typical example is $CH_3NH_3PbI_3$ (MA NH_3PbI_3), which has organic methylammonium cations located at the A-site, lead cations at the B-site and iodine at the X-site. In fact, inorganic-organic halide perovskite solar cell has been a hot topic in recent decades. Much effort has been paid to improve the energy transfer efficiency. The performance of halide perovskite solar cells has been fairly satisfying as it can even compete with single crystalline silicon solar cells. The main obstacles for the commercialization of perovskite solar cells are the stability problem and toxicity of lead [29].

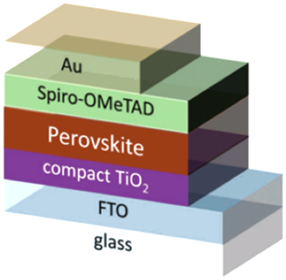

Figure 1.7 Architecture of perovskite solar cell device [29]

1.2.2 Oxide perovskite

Analogous to the definition of halide perovskites, oxide perovskites refer to perovskites with oxygen anions located at the X-site anions. The typical example of oxide perovskites is $CaTiO_3$, of which a face-centered cubic structure is shown in Figure 1.8

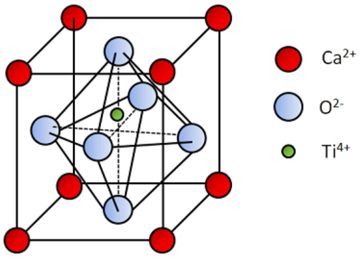

Figure 1.8 Structure diagram of $CaTiO_3$ [30]

The A-site and B-site cations should satisfy certain requirements to maintain the stability of the oxide perovskites. The first is the ionic radius. According to Goldschmidt[31], the radii of the cations, r_A and r_B, of a stable oxide perovskite should give a tolerance factor t (calculated using Eq 1.1) in the range of 0.75 and 1.

$$t = (r_A + r_O)/\sqrt{2(r_B + r_O)} \tag{1.1}$$

Specially, at value in the range of 0.95-1.0 is generally for perovskites with a cubic structure. A smaller t value (i.e., < 0.95) is for the perovskites with slightly distorted structure, while a larger t value (i.e., > 1.0) is for ferroelectrics [32].

Apart from ionic radius, the A-site and B-site cations should have correct valence to ensure the electroneutrality of the oxides. It means that the sum of the valences of the A-site and B-site cations should equal to the valence of oxygen anions in a unit cell. Therefore, the common form of oxide perovskites is $A^{1+}B^{5+}O_3$, $A^{3+}B^{3+}O_3$ or $A^{2+}B^{4+}O_3$.

1.2.2.1 Non-stoichiometry

In some specific conditions, the plethora of compounds will happen because of the substitution of A-site and B-site cations. In order to maintain the electroneutrality, A-site or B-site deficiencies, or oxygen vacancies will occur. This leads to "non-stoichiometry" in oxide perovskites [33]. Non-stoichiometry is one of the popular research directions related to oxide perovskites. It is the basis of heterogeneous catalysis. Apart from that, it is also closely related to ion conduction and superconductivity of materials.

1.2.3 Distortion of Perovskite structure

The structure and lattice parameters of oxide perovskites will vary significantly for different A-site and B-site cations. Apart from the types of the cations, the structure can also be modified by incorporating additional A-site or B-site cations with different sizes or valences. For instance, a new perovskite $AB_{0.5}B'_{0.5}O_3$ can be developed by replacing half of the B-site cation with another cation. Consequently, the unit cell of the newly developed oxide perovskite become doubled in length along the three axes. If the valences of the two B-site cations (i.e., B and B') are different, the oxygen anion will shift from its origin position towards the highly charged B-site cation which will make the lattice structure transform from cubic into orthorhombic, rhombohedral, tetragonal, monoclinic or triclinic [34]. In fact, distortion not only appears in perovskite oxides with multiple A-site or B-stie cations, it also exists in $CaTiO_3$, which was thought to be cubic before 1946 when Megaw [35] showed that it is actually orthorhombic.

Although distorted oxide perovskites do not possess an ideal structure as predicted, those deviations have not hindered the research work. In fact, some of the deviations from the cubic structure can enhance or induce certain properties and many researches have made use of them in new applications. Piezoelectricity, which is originated from the acentric symmetry of the lattice structure, is one of the most attracting phenomena in oxide perovskites.

1.2.4 Piezoelectricity of oxide perovskite

Although this thesis mainly discusses about mechanoluminescence, which refers to the energy transfer from mechanical load to optical energy, the discussion of piezoelectricity is also necessary. It is because some of the existing mechanisms models involve the participation of piezoelectric effect. To help the explanation of different mechanism models, the basic concept of piezoelectricity is introduced in this session.

Piezoelectricity refers to the inducement of electrical charges by mechanical stress (direct effect), or the generation of mechanical strain by an electric field (converse effect). Among the 32 crystal classes, 20 of them exhibit the piezoelectric effects due to their non-centrosymmetric characteristic [36]. All piezoelectric materials own a spontaneously polarization as their characteristic. Some of them exhibit the piezoelectric effect by nature, like quartz (SiO_2) while some of them need to be engineered by poling before exhibiting the piezoelectricity, like Pb (Zr, Ti) O_3 and $BaTiO_3$. Besides originating from the intrinsic non-centrosymmetric crystal structure, the piezoelectricity can exist in centrosymmetric compounds which have specific types of lattice defects or microstructures [9, 37, 38].

The intrinsic non-centrosymmetric materials that need to be engineered by poling before exhibiting the piezoelectricity are called ferroelectric materials. In general, they exhibit stronger piezoelectricity than those intrinsic piezoelectric materials [39]. Moreover, the direction of their spontaneous polarization can be switched by an external electric field. Ferroelectric materials have a wide range of applications, such as sensors and transducers.

1.3 Rare earth element

According to the type of the luminescent center, mechanoluminescence (ML) materials can be classified into two types: intrinsic ML materials and extrinsic ML materials. Intrinsic ML materials can exhibit ML by themselves, like loaf sugar and radiated alkali halides. Extrinsic ML materials, including ZnS: Mn^{2+} and SrAlO4: Eu^{3+}, need a dopant to work as the luminescent center. Rare earth elements are frequently used as the dopant due to their unique properties. The electron configuration of rare earth elements can be represented as $[Xe]4f^n6s^2$ or $[Xe]4f^{n-1}5d6s^2$, where [Xe] is the electron configuration of Xenon. The unfilled 4f shell enables rare earth elements able to generate various energy levels and absorb electromagnetic waves from infrared to ultra-violet (abbreviated as UV).

Depending on the host materials and the doping level, trivalent praseodymium (Pr^{3+}) dopant can emit light in blue or red regions. The energy level diagram of Pr^{3+} is shown below:

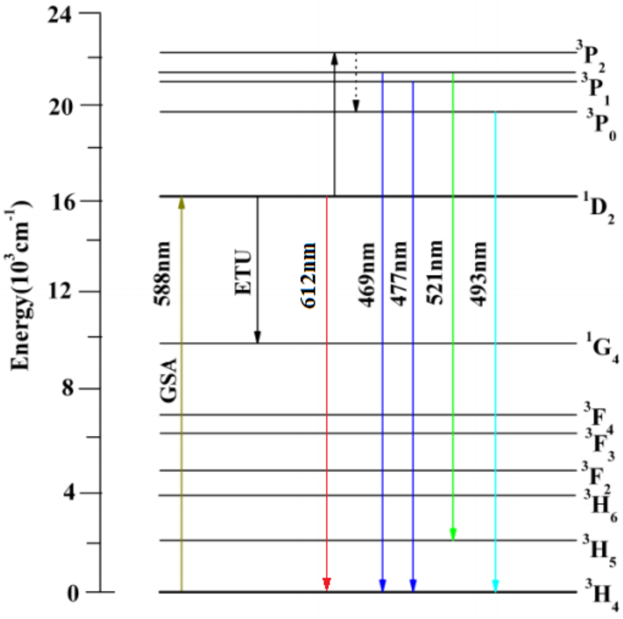

Figure 1.9 Energy level diagram of Pr in $4f^2 6s^2$ [40].

Unlike other rare-earth elements, an f-f transition, which is always forbidden, can be realized in Pr^{3+} ions. Electrons are relatively difficult to be excited to the 5d state of Pr^{3+} by any conventional optical stimuli since the state is generally between 40000 cm^{-1} and 60000 cm^{-1} [41]. For example, the excitation wavelength required for exciting electrons to the 5d state in $CaHfO_3$: Pr^{3+} is about 240 nm [42]. Therefore, the function of in Pr^{3+} as a luminescence center is basically originated from the energy transition inside $4f^2$ states. The red light induced by the $^1D_2 \rightarrow {}^3H_4$ transition is dominant in the material investigated in this thesis, $Ba_{0.15}Ca_{0.85}Ti_{0.9}Zr_{0.1}O_3$: Pr^{3+}. It has been shown that the red light emitted by Pr^{3+} doped in $CaTiO_3$ is based on the same energy level transfer.

The red light shows CIE color coordinates (0.680, 0.311) that is preferable for various applications [43]. However, according to the laser spectroscopy of Pr^{3+} conducted by many researchers, greenish-blue light is the dominant emission for most of the cases [41, 44]. As shown in the energy diagram (Figure 1.9), the greenish-blue light is resulted from the $^3P_0 \rightarrow {}^3H_4$ transition of Pr^{3+}, and partly from other transitions from the adjacent energy levels of $^3P_0$ to the $^3H_4$ ground state. It has been reported that $^3P_0$ greenish-blue luminescence is almost totally quenched to $^1D_2$ red luminescence through a non-radiative relaxation process in (Ba,Ca)TiO_3: Pr^{3+}[45]. Similar phenomenon has also been observed in $CaTiO_3$: Pr^{3+} [46]. The non-radiative relaxation has been explored by many researchers for developing an artificial color-control technique for further applications [47].

Many models have been proposed to explain this quenching phenomenon, such as he multi-phonon relaxation, cross-relaxation, intersystem crossing through low-lying excited state and intersystem crossing through the Pr-to-metal charge transfer state (CTS) [48-51]. Donega et al [52] have conducted a general study of the $^3P_0$ quenching in different Pr-doped compounds, in some which the quenching is negligible and in some of which the non-radiative relaxation is dominant. The number of phonons required to realize the quenching has also been taken into account for exploring the effect of multi-phonon relaxation. It has been concluded that in certain compounds, the strong covalency and relatively short Pr-ligand distance will result in a stronger electron-phonon coupling and consequently higher multi-phonon relaxation rates. For some other certain compounds, the intersystem crossing through low-lying 4f5d state is dominant. They have also claimed that the cross relaxation and intersystem crossing though CTS do not play a significant role in the quenching.

Among various mechanisms, the intersystem crossing through Pr-to-metal CTS model is most widely accepted mechanism for $CaTiO_3$: Pr. Boutinaud et al. have provided a reliable reasoning based on the analysis of energy band and crystal structure[46].], which does not agree with the intersystem crossing though low-lying 4f5d model proposed for explaining the quenching at that time and deduces the nonexistence of the low-lying 4f5d level in $CaTiO_3$: Pr. Based on the comparison with samples containing excessive Pr^{4+} ions, they proposed the charge transfer state (CTS) model. The model has been supported by EPR measurements in which an increase of paramagnetic $[Pr^{4+}$-Ti^{3+}-$O3]^+$ clusters is observed when the material is optically excited [53]. Although the CTS model has well been accepted controversy still exists especially when Zoila et al. have shown that the model is not sustained by ab initio calculation. They have also pointed out that all the evidences for the CTS model are not direct evidence [47]. Therefore, the explanation of the nonradiative transition in Pr^{3+} still cannot be drawn into a conclusion.

1.4 Relationship between ML and other luminescence

1.4.1 Electroluminescence (EL)

EL was firstly defined as the luminescence triggered by current flowing in an evacuated tube which containing inert gas. After the discovery of EL in dielectric phosphors, condensers composed of the phosphors and electrodes were developed. When an electric field is applied, it can produce a brief flash of light as a result of the recombination of electrons and holes. EL has found a wide application in solid state light emitting devices, like light-emitting diodes (LEDs). EL also includes the light emission resulted from the separation of two isolating surfaces which are originally held together [54]. During the separation, a discharge will happen and excite the surrounding gas, and thus inducing the luminescence. Since triboluminescence, a kind of mechanoluminescence, is also triggered by splitting or rubbing crystals, it has been considered consisting partially of electroluminescence. Therefore, EL is considered as a mixed light emissions from triboluminescence and excited ambient gas, which can be directly observed by comparing the spectra of surrounding gas and EL [55].

1.4.2 Persistent luminescence

Persistent luminescence refers to the luminescence lasted for an appreciable period of time after the exposure by high-energy radiation, like ultra-violet (UV) light. It is also known as phosphorescence or afterglow. Similar to ML and TL, the phenomenon of persistent luminescence is also related to charge carrier traps created by defects inside the materials. The long-time persistent luminescence is due to the slow releasement of trapped charge carriers induced by thermal energy absorbed from the external environment. Some of the popular ML materials, like ZnS: Cu^{+} and $SrAl_2O_4$: Eu^{2+}, also show persistent luminescence and have been put into commercialization for several decades [56, 57]. The most popular persistent luminescent material in early 21th century is $SrAl_2O_4$: Eu^{2+}, Dy^{3+}, which is also well known as a ML material [58]. Therefore, the mechanism model of persistent luminescence model might bring some inspiration for understanding the mechanism of ML.

1.4.3.1 Matsuzawa model

In 1996, Matsuzawa et al. developed a model to describe the working principle of persistent luminescence observed in $SrAl_2O_4$: Eu^{2+}, Dy^{3+} [58]. In the model, holes are assumed to be the main charge carriers in this material and the assumption has been supported by the Hall measurements conducted by other researchers [59]. As illustrated in Figure 1.10, electrons of Eu2+ ions are firstly excited by UV light to the excited state. Some of the holes (formed in Eu^{2+} ions) may escape to the valence band, which are then captured by Dy^{3+} ions in forming Dy^{4+} ions. The thermal energy from ambient environment would de-trap the holes and let them release to the valence band again. If enough thermal energy from the ambient environment is absorbed, the holes (trapped in Dy^{4+} ions) can be de-trapped and released back to the valence band, which will finally allow the electrons in the excited state of Eu^{+} ions to relax back to the ground state with the emission of photons.

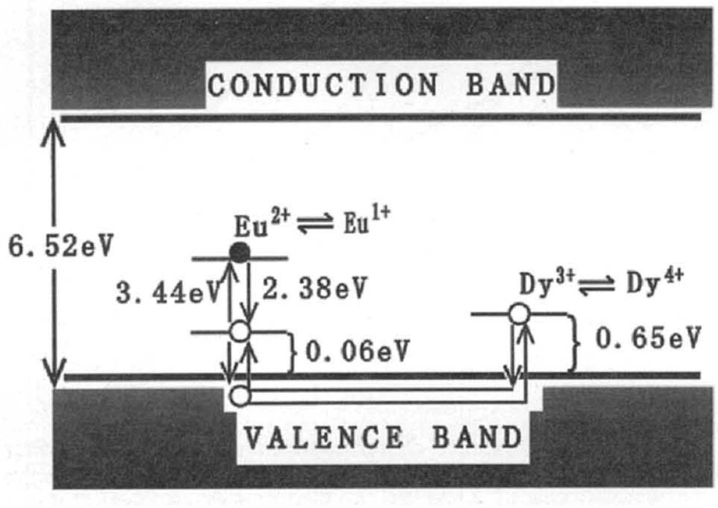

Figure 1.10 Matsuzawa model

The Matsuzawa model has been widely used to explain the observed persistent luminescence in newly discovered materials. However, no experimental evidence, in particular for the formation of the chemically unstable Eu^{+} and Dy^{4+} ions, have been provided for validating the model.

1.4.3.2 Aitasalo model

Aitasalo et al. brought out another mechanism model with some modification of Matsuzawa model in 2003 [60]. Since the Matsuzawa model was built to explain the persistent luminescence in co-doped $SrAl_2O_4$: Eu^{2+}, Dy^{3+}, it cannot be used to explain the persistent luminescence in $SrAl_2O_4$: Eu^{2+}, in which no interaction between the co-dopants exists. It indicated that the co-dopant cannot play an explicit role in the persistent luminescence, i.e., it is just regarded as a source of trap levels rather than having a irreplaceable function. Based on this assumption, Aitasalo et al. suggested that the electrons in the valence band can be directly excited to trap levels with no specific origination (Figure 1.11). Different from Matsuzawa, Aitasalo model was built based on $CaAl_2O_4$: Eu^{2+}, Dy^{3+}. Holes are then produced (in the valence band) and caught by calcium vacancies. After absorbing the thermal energy from the ambient environment, the trapped electrons are released from the trap levels, migrate to oxygen vacancy trap, and then recombine with the holes caught by the cation vacancies. The energy generated from the recombination is directly transferred to excite the luminescence centers (e.g., Eu^{2+}), which will then relax back to the ground state with the emission of photons. Similar to the Matsuzawa model, only holes will move as free charge carriers, and the electrons (released from the trap levels) will not be triggered to the conduction band.

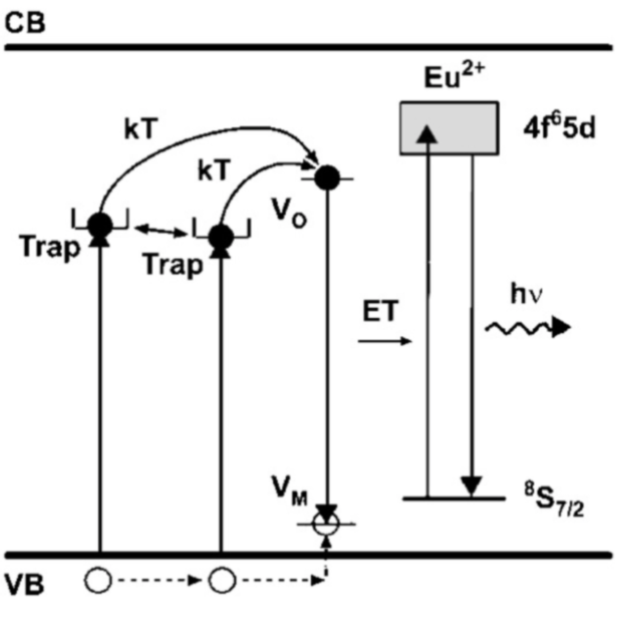

Figure 1.11 Aitasalo model in $CaAl_2O_4$: Eu^{2+}, Dy^{3+}

Unlike the Matsuzawa model, the generation of the chemically unstable Eu^+ and Dy^{4+} ions are not required in the Aitasalo model. The model is also applicable to the co-doped materials, in which the other co-dopant will have no explicit function in the whole process except to generate excessive lattice defects.

The Aitasalo model has been used to explain the weakening of persistent luminescence observed in compounds co-doped with Sm^{3+}. The co-doping of Sm^{3+} will lower the number of cation vacancies because of the reduction to Sm^{2+} during the fabrication. The model can also be used to explain the 430-nm persistent luminescence induced in $CaAl_2O_4$: Eu^{2+}, Dy^{3+} by the irradiation of 530-nm visible light.[61].

Nevertheless, the Aitasalo model has a limitation, i.e., the assumption of the close proximity between defects and luminescence centers. Without this, the direct transfer of the energy generated from the recombination of the electrons (released from the trap levels) and holes (caught by the cation vacancies) to the luminescence centers for excitation and then light emission cannot be realized.

1.4.3.3 Dorenbos model

In both the Matsuzawa and Aitasalo models, holes are assumed to be the main mobile charge carries, which was not agreed by Dorenbos et al.[62, 63]. In the Dorenbos model (Fig. 1.12), after the excitation of Eu^{2+}, electrons will escape to the conduction band since the 5d level of Eu is close to the conduction band. As a result, Eu^{3+} ions are produced. The free electrons will then be trapped by the co-dopant Dy^{3+} ions and Dy^{2+} ions are formed. When thermal energy is absorbed, the trapped electrons will be released, return to the Eu^{3+} luminescent center, and then relax back the ground state with the emission of light.

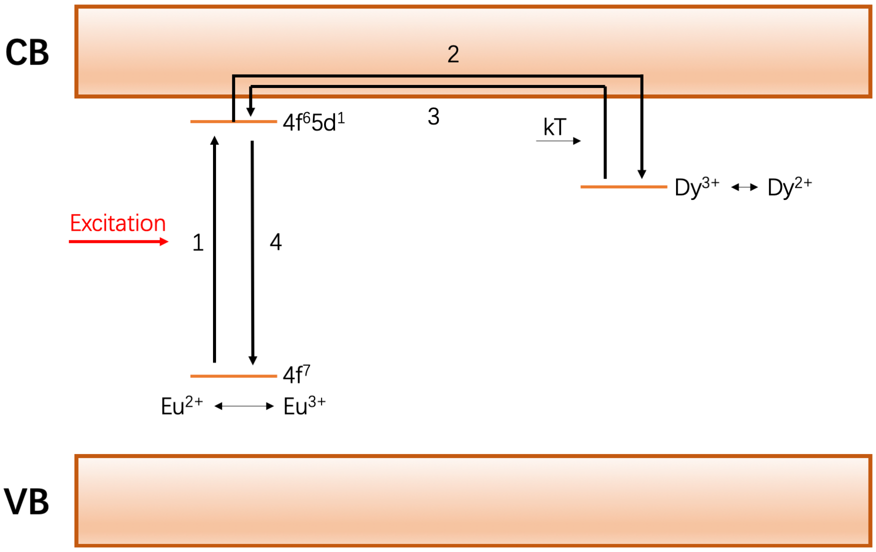

Figure 1.12 Dorenbos model

Similar to the Matsuzawa model, this model cannot be used for singly doped materials. The contribution of the Dorenbos model is the assertion of electrons as mobile charge carriers.

1.4.3.4 Clabau model

Clabau and his groupmates have found that the number of Eu^{2+} ions decrease significantly during the excitation and then increases obviously after the exposure. This suggests that Eu^{2+} ions have participated in the trapping process, which is not consistent with the Aitasalo model. In the Aitasalo model, the energy transfer to Eu^{2+} occurs only after the trapping of charge carriers. They have also found that, based on the photoconductivity measurements, no free charge carriers are produced in $SrAl_2O_4$:Eu^{2+}, Dy^{3+} under UV excitation around 300 K; but the thermoluminescence measurements reveal de-trapping processes at similar temperatures. Therefore, the assumption of producing free charge carries suggested in both the Matsuzawa and Dorenbos models is not valid.

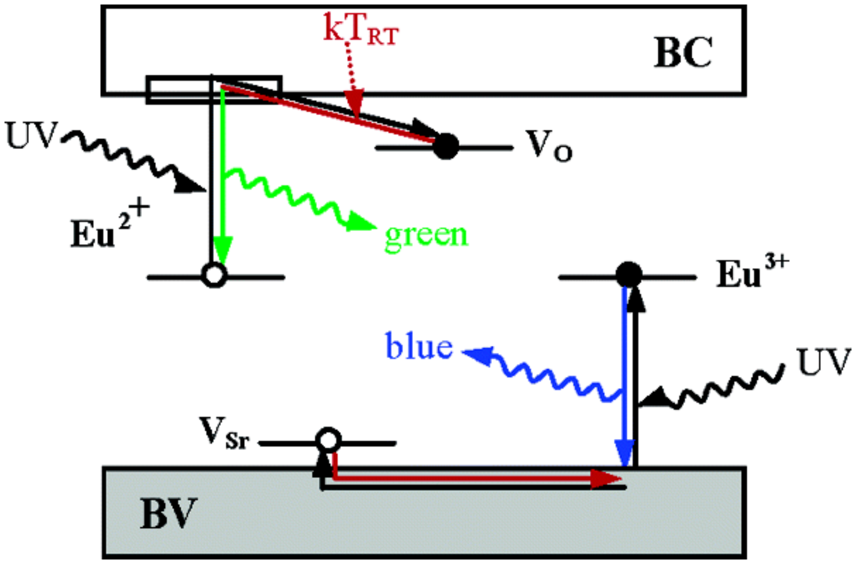

Figure 1.13 Clabau model in $SrAl_2O_4$: Eu^{2+}, Dy^{3+}

Similar to the Aitasalo model, an assumption of close proximity between luminescence centers and defects is also required in the Clabau model, since no free charge carriers will be produced during the whole process. Different to the Dorenbos model, only intrinsic defects, such as oxygen vacancies and cation vacancies, are suggested to be the defects participating in the trapping processes. This means that the co-dopants will not function as charge carrier traps in the persistent luminescence process.

This assumption is proved by the thermoluminescence measurement. The thermoluminescence glow curve showed the peaks of singly doped and co-doped samples only differ in size and location. The shape of peaks did not change obviously (Fig 1.14). The co-dopants can stabilize oxygen vacancies. Some co-dopants with lower ionization potential will attract oxygen vacancies more strongly, causing an increase in the depth of the traps and the lasting time of persistent luminescence. luminescence might increase.

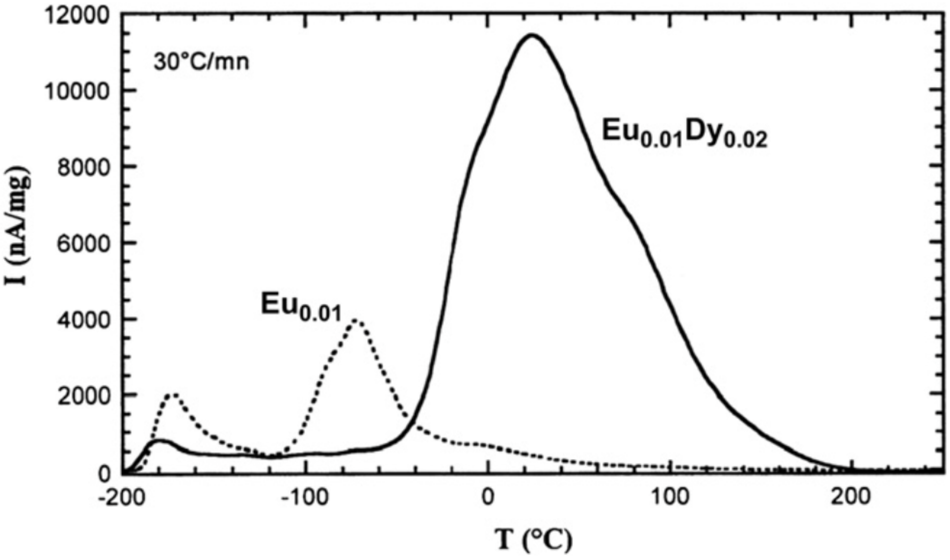

Figure 1.14 Thermoluminescence glow curves of singly doped $SrAl_2O_4$: Eu^{2+} and co-doped $SrAl_2O_4$: Eu^{2+}, Dy^{3+}

After reviewing different mechanism models of persistent luminescence, it can be seen that the transition of energy, types of traps and role of co-dopant are the most controversial parts. They are also the controversial parts for ML. Indeed, the transferring process of mechanical energy to the host lattice and the effects of the mechanical loads are more complicated, which makes the development of new ML materials more difficult.

1.4.3 Thermoluminescence (TL)

The emission time of persistent luminescence is highly dependent on the temperature of surroundings, so the emission intensity will change when the temperature changes, and this phenomenon is named as thermoluminescence. Apart from charge carriers released from traps involved in persistent luminescence, TL can release charge carriers in deeper traps when the temperature is high enough. Therefore, thermoluminescence can provide information of all the different traps levels in the compound. The connection between TL and ML has been investigated since certain materials were discovered to emit light when heated or scratched. It has been shown in the work of Wedwood et al. there is a certain parallel between these two kinds of luminescence[64]. However, it has been reported that some samples show a decrease of ML intensity after heating while some samples exhibit opposite phenomena [65]. It is well accepted that both TL and ML are triggered by the release of trapped charge carriers, which is induced by the thermal energy and mechanical load, respectively. In fact, the information of trap energy can be determined from thermoluminescence glow curve. The measurement of TL glow curve is included in this thesis and the principle of the TL measurement will be introduced in more details in Chapter 2.

1.5 Work scope

This work aims to develop a new ML material, i.e., $Ba_{0.15}Ca_{0.85}Ti_{0.9}Zr_{0.1}O_3$: Pr^{3+} (abbreviated as CBTZ-Pr) and to investigate the ML mechanism. The development of CBTZ-Pr is motivated by the good phosphor property of $CaTiO_3$: Pr^{3+} and the strong piezoelectricity of $Ba_{0.85}Ca_{0.15}Ti_{0.9}Zr_{0.1}O_3$. It is commonly known that $CaTiO_3$ has an orthogonal structure but no piezoelectricity. Inspired by the strong ML emission of ZnS:

Mn^{2+} [25], the piezoelectricity may help to release the trapped electrons and consequently induce a stronger ML. Therefore, we chose $Ba_xCa_{1-x}Ti_yZr_{1-y}O_3$: Pr^{3+} rare earth element doped perovskite trying to combine the high piezoelectricity of $Ba_{0.85}Ca_{0.15}Ti_{0.9}Zr_{0.1}O_3$ and strong red luminescence of $CaTiO_3$: Pr^{3+}. As a preliminary result, intense EML has been discovered in $Ba_{0.15}Ca_{0.85}Ti_{0.9}Zr_{0.1}O_3$: Pr^{3+} (CBTZ-Pr). However, different from our expectation, CBTZ-Pr shows naturally originated di-phase microstructure and neither of the phase is piezoelectric. This phenomenon had inspired us to propose a model to explain the non-piezoelectric ML.

In this project, we will explore the ML properties of CBTZ-Pr, in which the perovskite structured $Ba_{0.15}Ca_{0.85}Ti_{0.9}Zr_{0.1}O_3$ oxide serves as the host lattice and Pr^{3+} ions act as the luminescence center. The ML emission/phenomenon will be photographed for demonstration. The EML responses will also be examined via the application of a tensile stress, and the dependence of the emission intensity on the tensile stress will be investigated in detail. The repeatability or recoverability of the ML response will be investigated via the application of cycling tensile stress. The ML spectrum will be compared with the PL spectrum with the purpose of investigating the energy transfer processes.

The morphology and crystal structure of the sample will also be explored for investigating the relationship with the ML responses. In perovskite structure CBTZ-Pr oxide, co-existence of different phases may occur, and the composition and distribution of those phases may have significant effects on the light emitting processes.

The thermoluminescence behavior of the sample will be examined for investigating the charge trapping centers, in particular their positions in the energy band structure. Based on the results, a model will be proposed to elucidate the mechanism of the observed EML phenomenon.

Chapter 2 Methodology

2.1 Preparation of CBTZ-Pr

2.1.1 Preparation procedure of the CBTZ-Pr ceramics

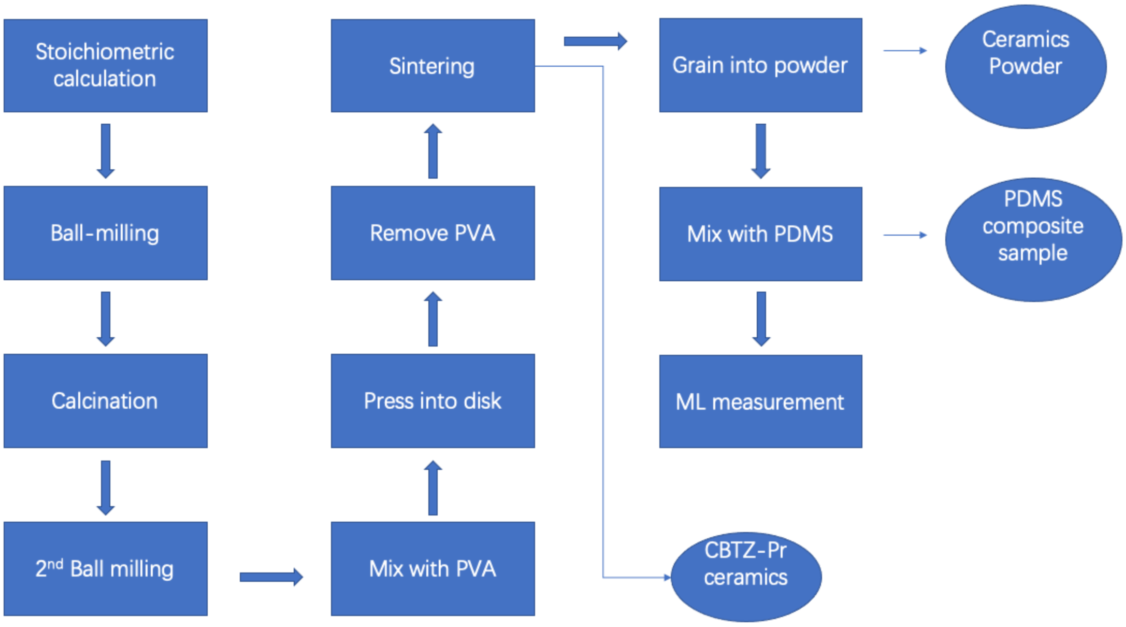

Figure 2.1 Flow chart of sample fabrication procedure

The CBTZ-Pr ceramics were prepared by a solid-state reaction method. The raw materials used to prepare the ceramics are $BaCO_3$ (99.5% purity), $CaCO_3$ (99% purity), TiO_2 (99.9% purity), ZrO_2 (99.9% purity) and Pr_6O_{11} (99.9% purity). First, the weights of various raw materials were calculated according to the composition of the ceramics. Then the raw materials were mixed with ethanol alcohol, and ball-milled thoroughly for 12 hours using zirconia balls. After the ball milling, the mixture was dried at 120°C and calcined at 1200°C in air for 2 hours. During the calcination, the ions interact with each other through the inter-diffusion process and form a chemically and crystallographically uniform structure [66]. The calcined powders were then ball-milled again for 12 hours. After drying, the powers were sieved through an 80-mesh screen and mixed with a polyvinyl alcohol (PVA) binder solution (5 wt%). The mixture was then pressed into pellet under ~500 MPa pressure. After burning out the binder at 650°C, the samples were sintered at 1350°C for two hours in air.

2.1.2 Fabrication of CBTZ-Pr/PDMS sample

Polydimethylsiloxane (PDMS) is one of the most frequently used silicon-based organic polymers with its good flexibility. The advantages of PDMS, including low cost, fast manufacture, optically clear over a wide range of visible light make it have high potential in various industries. It is widely used as a substrate material and has practical application in microfluidic systems. The low shrinkage rates also make it useful in soft lithography technique [67].

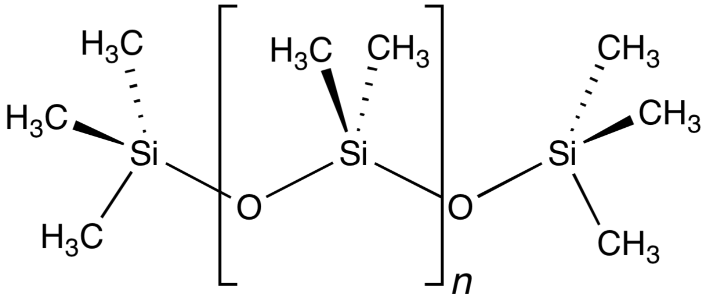

Figure 2.2 Structure diagram of PDMS

Due to its mechanical property, PDMS is frequently used as elastomeric substrate materials combined with other substance. Among various commercial PDMS products, Sylgard 184 silicone elastomer (Dow Corning) is highly reliable and used in various academic research. The Sylgard 184 silicone elastomer kit consist of two components: the silicone elastomer base and silicone elastomer curing agent. The curing agent induces cross-linking of PDMS to form a tridimensional polymetric network. The curing process is called sulfur vulcanization and is commonly used in fabrication of rubber. The properties of Sylgard 184 silicone elastomer have been investigated by Johnston et al, including the effects of the curing temperature on elasticity, compression and hardness [68].

The ceramic samples fabricated following the procedures listed in Figure 2.1 were used to prepare composite samples with a matrix of PDMS. The sintered ceramics were first ground into powders and sieved through a 600-mesh screen, and then mixed with the PDMS in weight ratio of 7:3 thoroughly. The PDMS was prepared in advance by mixing the elastomer base and the curing agent in a ratio of 10:1. The mixture was then heated at 90°C for curing.

The flexibility of the PDMS matrix makes the transfer of the external mechanical stress to the ceramic powders feasible and effective. It also enables large and reversible deformation of the sample without breakage, which is difficult to be achieved in ceramics samples. The mechanical property of the PDMS matrix can be adjusted by changing the curing temperature or the ratio of the elastomer base to the curing agent. In addition, the PDMS elastomer is optically transparent down to 240 nm, which make no influence on the measurement of light emission. Therefore, it is suitable for the fabrication of the composite ML sample.

2.2 Characterization of CBTZ-Pr

2.2.1 Characterization of crystalline structure

2.2.1.1 XRD (X-ray diffraction)

XRD is frequently used in material science to determine the atomic and molecular structure of crystal. Crystalline structure refers to a long-range systematic arrangement of atoms or ions. Due to this characteristic, crystal contains many planes, and those planes are separated by a specific distance. Atoms in the crystal may work as centers of x-ray scattering and are able to diffract x-rays when the wavelength of the x-rays and distance between the planes satisfy follow Bragg's law [69].

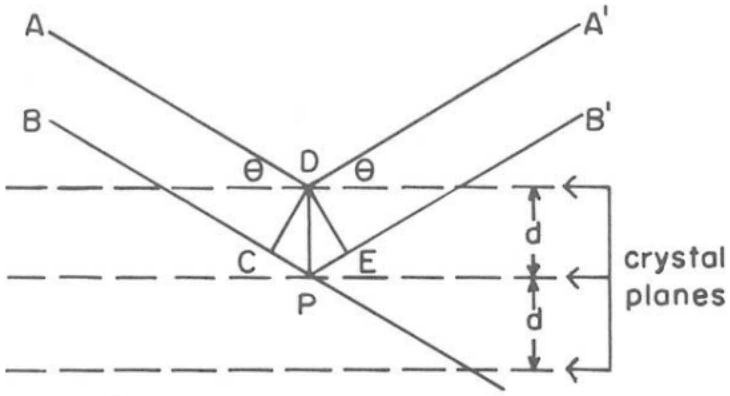

Figure 2.2.1.1 Principle of XRD in crystal [70]

λ refers to the wavelength of x-ray, which is 0.154 nanometer in this thesis (CuK_α). The XRD measurement in this work was conducted using an x-ray diffractometer (SmartLab 9 kW-Advance, Rigaku Co., Japan). In the measurement, the sample was irradiated with an x-ray beam having a wavelength λ of 0.154 nm (CuK_α radiation) at various incident angles θ. The x-rays scattered from different crystal planes (with an inter-distance of d) interfere with each other, giving a variation of intensity with θ (scattering angle) or a diffraction spectrum. Constructive interference or diffraction peaks occur at θ satisfying Bragg's law:

$$n\lambda = 2d\sin\theta \tag{2.1}$$

2.2.2.2 Back-scattered Scanning Electron Microscope (BSE)

Scanning Electron Microscope (SEM) is frequently used in material morphology to observe the surface morphology of materials. It produces images of the materials by scanning their surface with focused beam of electrons. It can present the surface topography and composition information of the materials, for instance, the crystallinity which can be reflected from the size of grains shown in SEM. Back-scattered electrons (BSE) are produced by elastic scattering of incident electrons with the materials. The BSE signal’s intensity significantly depends on the atomic number of the materials, which can be used for differentiating regions with different chemical compositions. However, BSE cannot accurately identify the element composition of these regions. Therefore, energy dispersive x-ray spectroscopy is also needed for element identification.

In this work, BSE was used to recognize different phases existing in the CBTZ-Pr ceramics. The BSE microscopy was conducted by using a tungsten thermionic emission SEM system (TESCAN VEGA 3, TESCAN, Czech Republic).

2.2.2.3 Energy dispersive x-ray spectroscopy (EDS)

EDS is an analytical technique for analyzing chemical composition. It is based on the interaction between x-rays and atoms of the materials. When atoms are irradiated by x-rays, an electromagnetic emission spectrum with a unique set of peaks will be produced [71], based on which the chemical compositions can be well characterized.

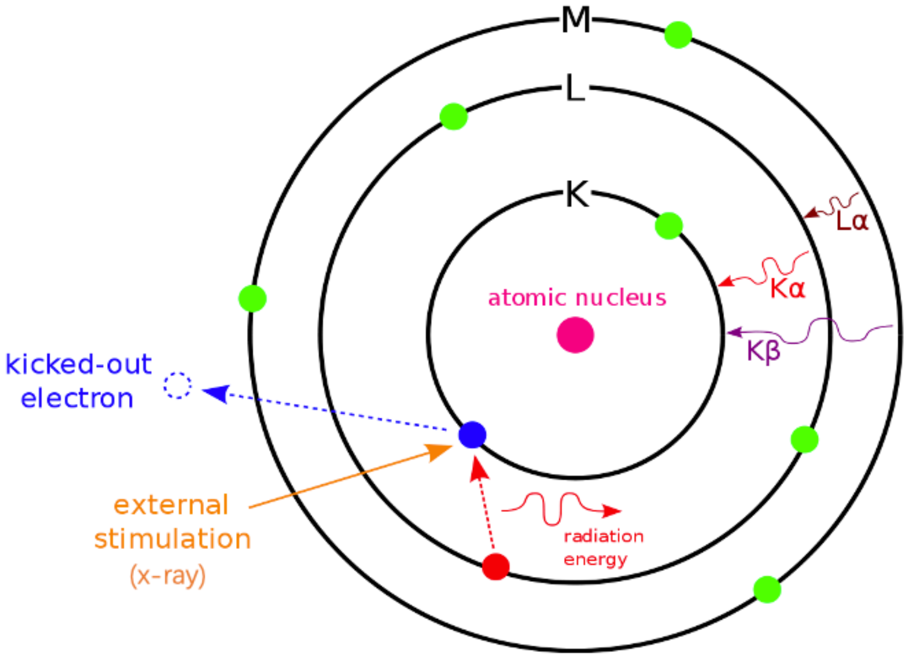

Figure 2.4 Schematic diagram of interaction between X-ray and atoms [72]

As shown in Figure 2.4, the incident x-ray will kick out an electron in inner electron shells and create an electron hole. The electron located in inner shells owns lower potential energy compared to outer shell electron. Therefore, when there is a hole in lower-energy levels, the outer-shell electron will transit to the inner shell and release a photon with energy the same as the difference between the two energy levels. Accordingly, the emitted photons can only have certain energies, forming a characteristic emission spectrum which is unique for the material[73].

In this thesis, EDS was used to analyze the chemical compositions of the phases identified by BSE. The EDS spectrum was measured using a tungsten thermionic emission SEM system (TESCAN VEGA 3, TESCAN, Czech Republic).

2.2.3 Measurement of ML

2.2.3.1 ML image recording

An ML image system has been developed to record the ML responses of the CBTZ-Pr/PDMS composite samples. The schematic diagram of the system is shown in Figure 2.5. A tip driven by an electromagnet is used to apply a force on the composite thin films, which is sticked on a glass plate. The electromagnet is connected to the collector of a transistor and the positive pole of a DC voltage source. The gate of the transistor is connected to an oscillator, which can then turn the electromagnet on or off.

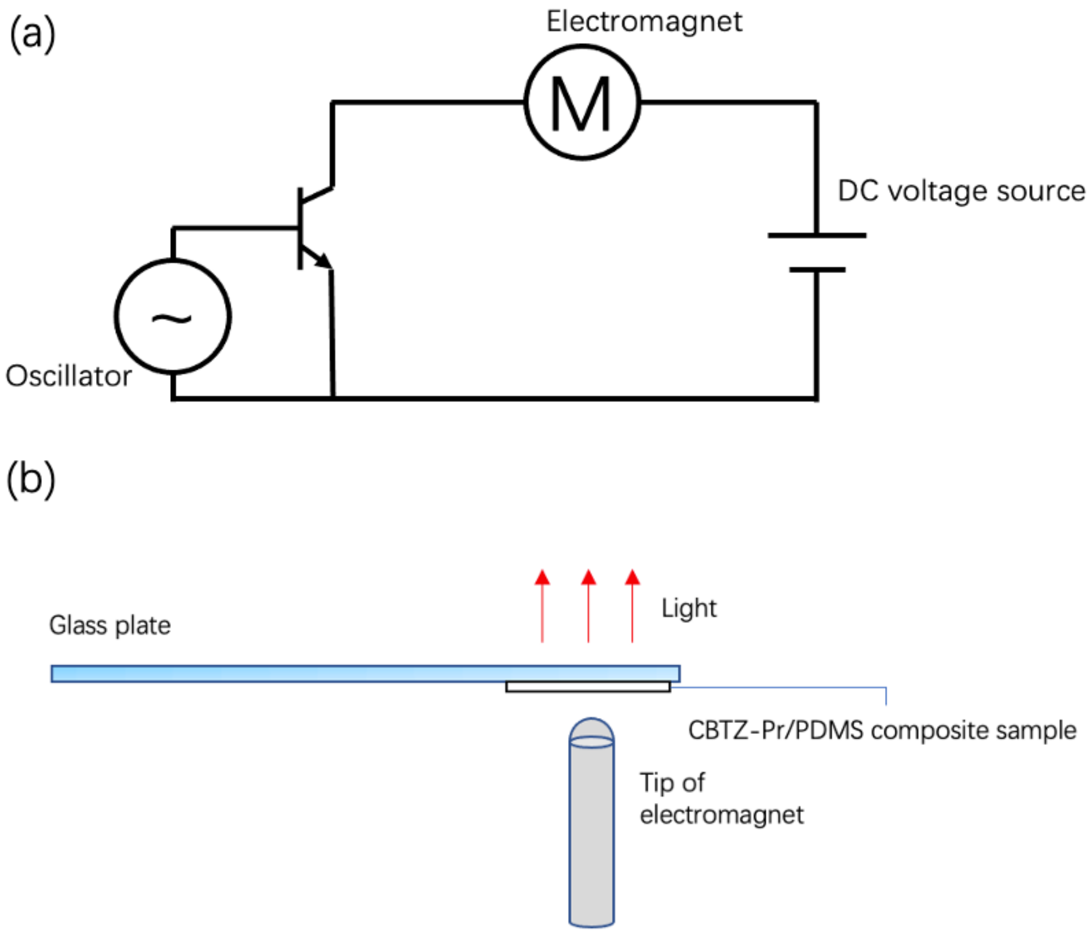

Figure 2.5 Schematic diagram of measurement system (a) and Detail in mechanical load on specimen (b)

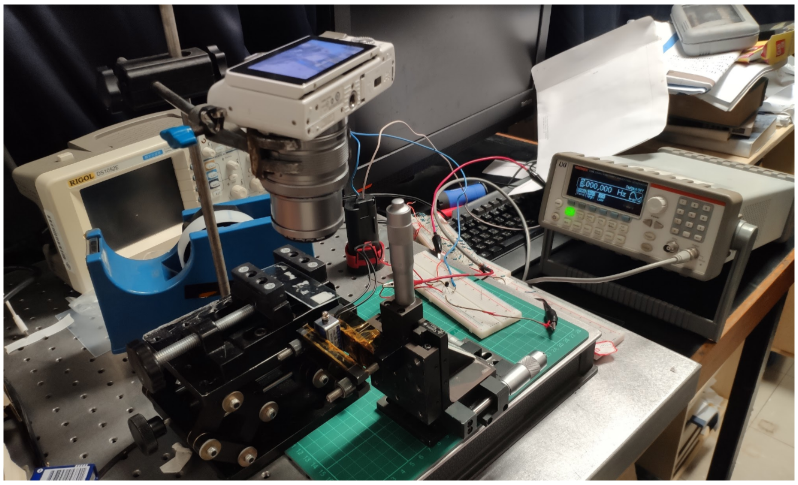

Figure 2.6 Photo of ML measuring system

As shown in Figure 2.6, a camera is positioned above the glass plate, below which the composite sample is attached. The thickness of the composite sample is about 100 μm, so that the ML emission can transit through the sample and reach the camera for the measurement. The measurement is taken place in a dark environment without any ambient light. Before each measurement, the sample was exposed to a UV light of wavelength 365 nm for 1 min for recovery.

2.2.3.2 ML Data recording

The ML emission intensity was measured using a photomultiplier tube (PMT, H11890, Hamamatsu, Japan). The CBTZ-Pr/PDMS composite sample was shaped into stripes with length of 6cm and cross area of 1mm^2. It is placed between two holders, one of them is movable and another one is stationary. During the experiment, the sample is stretched by moving one of the holders. The PMT placed above the sample will collect the light emitted from the sample. The schematic diagram of the system is shown in Figure 2.7.

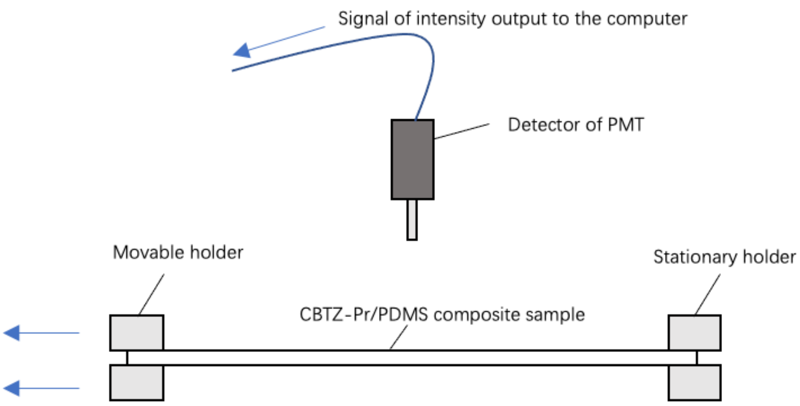

Figure 2.7 Schematic diagram of ML intensity measurement

Both the ML and PL emission spectra were measured using a fiber optic spectrometer (USB2000+, Ocean Optics, USA). The schematic diagrams of the measurements are shown in Figure 2.8. Similar to Emission intensity measurement, the spectrum of ML is also collected when the CBTZ-Pr/PDMS sample is stretched by external force. The PL spectra is gained when the sample is irradiated with UV light (365nm).

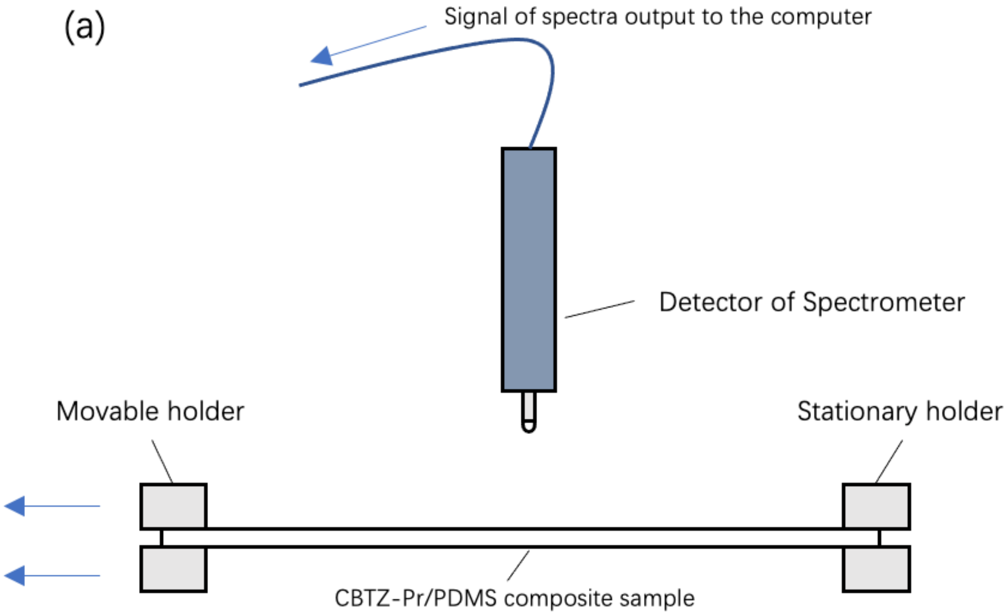

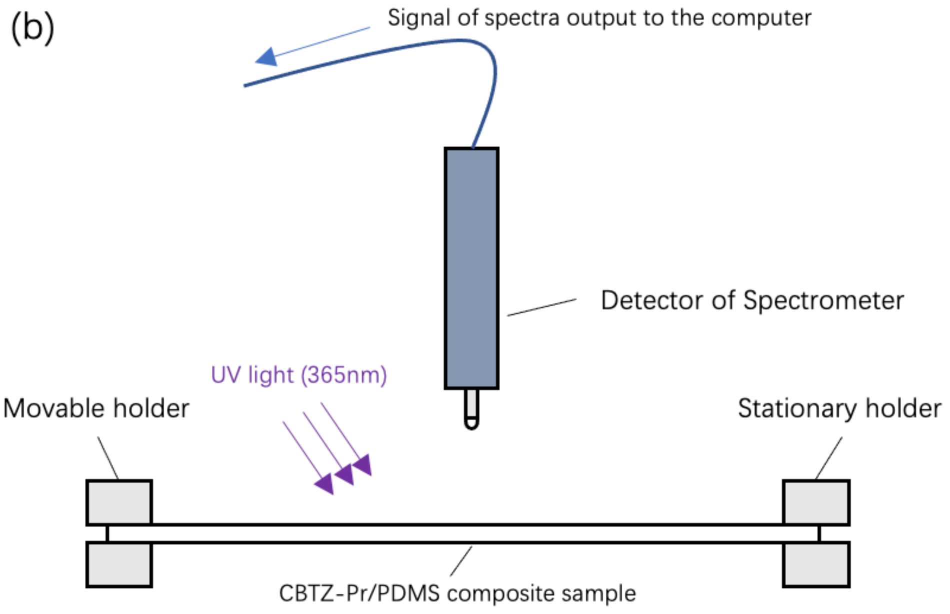

Figure 2.8 Schematic diagram of (a)ML and (b)PL spectra measurement

2.2.4 Thermoluminescence

Thermoluminescence (TL) refers to the emission of light due to thermal energy. As discussed in Chapter 1, the external stimuli to trigger the luminescence can be of various types, including thermal energy. A large number of photons may be released from materials at a specific temperature, and thus producing a peak in light intensity. A glow curve is then obtained by plotting the light intensity as a function of temperature. In fact, the shape of the glow curve highly depends on the traps levels existed in the materials[74]. TL also has found applications in dosimetry, radio biology, medicine, etc. [75, 76], and those applications are generally closely related to the trapping-emitting process in TL materials. In order to understand the TL response, it is needed to evaluate the kinetic parameters related to the trapping-emitting process. The most significant parameters are the activation energy of the traps, E (in eV) and the frequency factor, s (in s^{-1}). The relationship between E and s is determined by the order of kinetics in the de-trapping process.

2.2.4.1 1st order kinetics

For 1st order kinetics, no re-trapping will occur and the TL intensity is proportional to the rate of change in the concentration of trapped electrons [77]. The equation fir the 1st order kinetics is given as:

$$I = -c\left(\frac{dn}{dt}\right) = cs\ exp\left(-\frac{E}{kT}\right)n \qquad (2.2)$$

where I is the TL intensity, n is the concentration of trapped electrons, T is the temperature in K, k is Boltzmann's constant and c is a proportionality factor. In general condition, the proportionality factor, c can be considered as unity without any loss [77]. The frequency factor, s is independent of E for 1st order kinetics. Based on analytical deduction, Randall and Wilkins have proposed a relationship between E and s in 1st order kinetic cases[77].

$$\frac{\beta E}{kT_m^2} = s\ exp\left(-\frac{E}{kT_m}\right) \qquad (2.3)$$

where β is the increasing rate of temperature and T_m is the temperature with maximum TL intensity. The relationship is highly useful as it relates the trap energy directly to the frequency factor. Since the first activation energy estimation was given by Urbach in 1930 [78], many calculation methods have been proposed [79-83]. In this work, the calculation method based on the total half-width proposed by Chen et al. was used [84].

2.2.4.2 2nd order kinetics

The relationship between the TL intensity and the concentration of trapped electrons has also been evaluated by Garlick and Gibson, given as [79]:

$$I = -\frac{dn}{dt} = s^{'} n^{2} exp\left(-\frac{E}{kT}\right) \qquad (2.4)$$

Equation 2.4 implies that s', which is the derivative of s with respect to time, is independent of E for 2nd order kinetics. The main difference between the 1st and 2nd order kinetics is the probability of re-trapping. When the probability of re-trapping is equal or larger than that of recombination, 2nd order kinetics will occur while for 1st kinetics, the probability of re-trapping is assumed to be 0 [85, 86].

2.2.4.3 Determination of kinetics order

It is important to determine the kinetics order of TL peaks. Halperin et al have introduced a method for determining the kinetics order[81]. In the method, a parameter μ_g which is introduced and defined as n_m/n_0, where n_m is the concentration of trapped electrons at T_m and n_0 is the initial concentration, is introduced [81]. In practice, it is approximated as $(T_2-T_m)/(T_2-T_1)$, where T_1 and T_2 is the 2nd and 2nd value of temperature with half of maximum TL intensity, respectively, and Tm is the temperature with maximum TL intensity. Generally, the value of μ_g is around 0.5. When the trap level is within the forbidden gap, the activation energy E can be estimated as:

$$E = (\frac{q}{\delta})kT_m^2 \tag{2.5}$$

where the $\delta = T_2 - T_m$, q is a value depending on the kinetic order. For the 1st order kinetics, $q=1.72\mu_g(1-1.58\Delta)/(1-\mu_g)$ and for the 2nd order kinetics, $q=2\mu_g(1-2\Delta)/(1-\mu_g)$. Δ is a correction factor, its relationship with E is shown in Equation (2.6).

$$\delta = \frac{2kT_m}{E} \tag{2.6}$$

By combining Equation 2.5 and 2.6 together, a relationship between q and Δ is gained.

$$\frac{2}{\Delta} = \frac{T_m}{\delta} q \tag{2.7}$$

In equation 2.7, T_m and δ are constants determined by TL glow curve. Depending on the kinetic order, q can be accordingly replaced by μ_g and Δ by two equations. μ_g can be considered as a constant with value of 0.5. As a result, two quadratic equations of Δ can be obtained.

$$-2\Delta^2 + \Delta = \frac{\delta(1-\mu_g)}{\mu_g T_m} \tag{2.8a}$$

$$-1.58\Delta^2 + \Delta = \frac{\delta(1-\mu_g)}{0.86\mu_g T_m} \tag{2.8b}$$

By pre-assuming the kinetics order, check whether the value of Δ satisfy the condition corresponding to the assumption, i.e., if Δ solved from Equation 2.8a satisfy $\mu_g \approx (1+\Delta)/e$, the peak belongs to 1st order kinetics. Similarly, if Δ of Equation 2.8b is around $(1+\Delta)/2$, the peak is 2nd order kinetics.

It has been shown that the 1st order kinetics generally appear in semiconducting crystals [87], where the traps and luminescence centers are adjacent to each other [88]. Accordingly, it is suggested that 1st order kinetics also appear in CBTZ-Pr. In order to ensure the conclusion, the calculation will be conducted in part 3.4 to show the order of kinetics

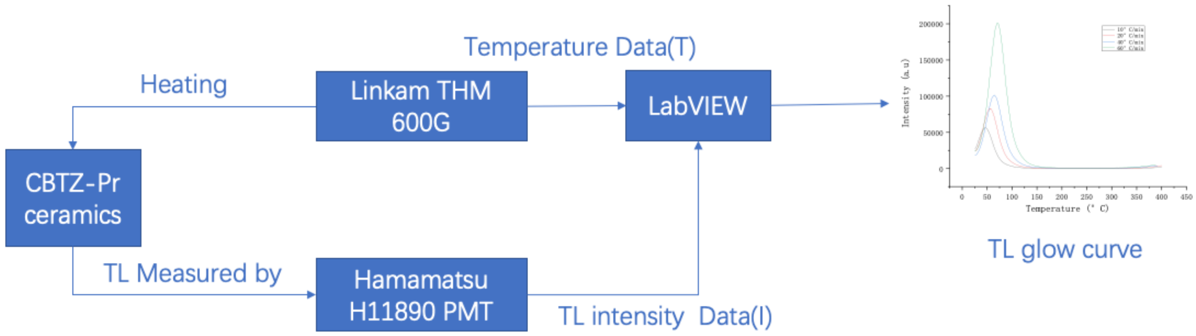

Figure 2.9 TL measurement system

An experimental setup was developed for measuring the TL glow curves. The diagram pf the measurement is shown in Figure 2.9. A heating stage (Linkam THM 600G) is used to increase the temperature of the sample from 25°C to 400°C at different rates and a photomultiplier (PMT, H11890, Hamamatsu, Japan) is used to measure the emission intensity.

Chapter 3 Red-Colored Mechanoluminescence emission in $Ba_{0.15}Ca_{0.85}Ti_{0.9}Zr_{0.1}O_3$: $0.2Pr^{3+}$

3.1 ML phenomenon recording

3.1.1 ML images

3.1.1.1 Images of pressure triggered ML

Before the ML measurements, the CBTZ-Pr/PDMS composite sample was irradiated with UV light (365 nm) for 1min. After the exposure, the sample emitted a red afterglow emission for about 10 min. For the photograph taking, the shutter duration of the camera was set as 10 s to capture the ML emissions during the period. A periodic compressive force at 1 Hz was exerted to the sample using the system described in Chapter 2. The frequency of 1 Hz was selected to avoid heating of the sample by the mechanical load. Figure 3.1 shows the photos of the composite samples with and without the application of compressive stress, respectively.

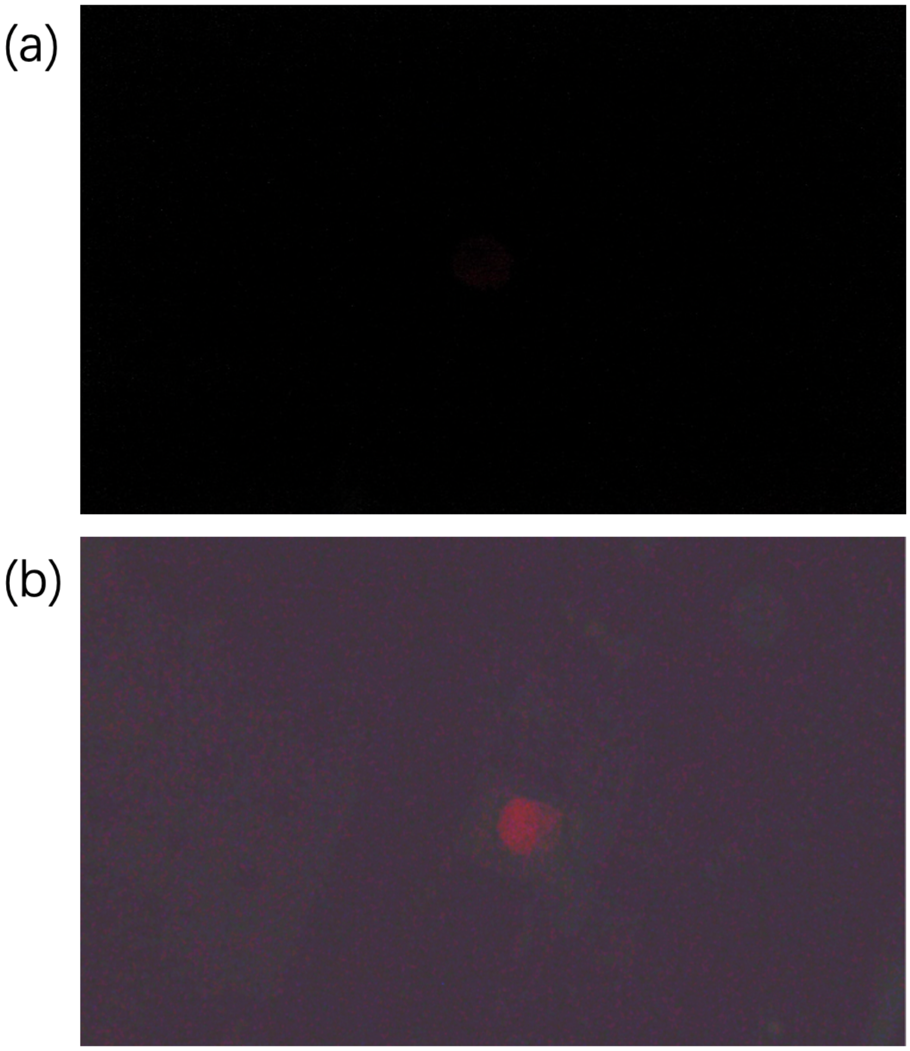

Figure 3.1 Photograph of CBTZ-Pr/PDMS composite sample (a)before and (b) after the application of pressure

As shown in Figure 3.1, when subject to the mechanical stress, the sample emits red light which can be observed by the naked eye and captured by camera. However, as the compressive stress is removed, no red light is observed, suggesting that the duration of ML emission is short, and the luminescence process terminates quickly after the application of the stress.

3.1.1.2 Images of friction force triggered ML

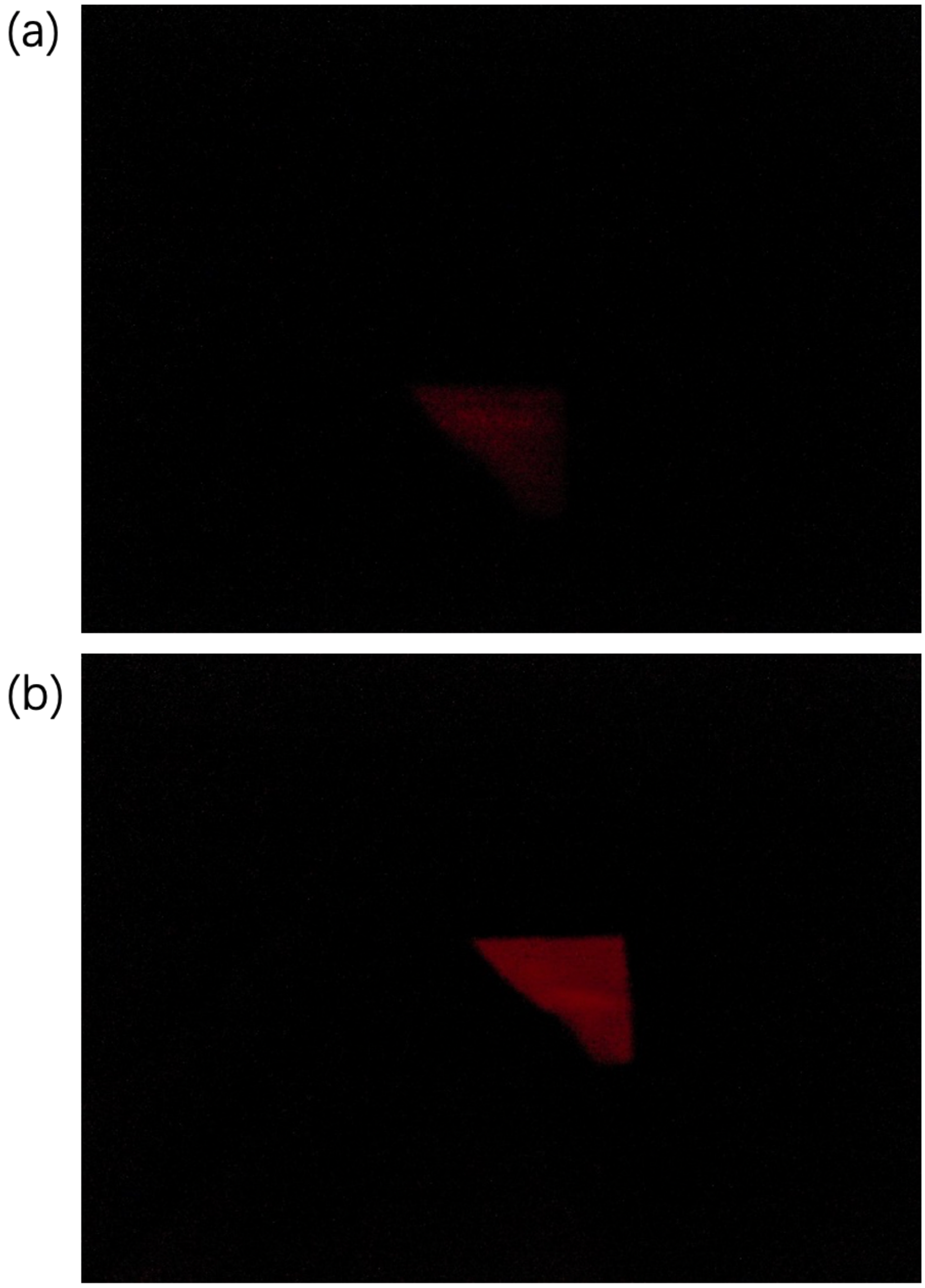

Figure3.2 Photograph of ML with friction force with intensity of afterglow existing (a) low and (b) high

As shown in Figure 3.2, the ML emission of the composite sample can also be triggered by a frictional force. Similarly, the CBTZ-Pr/PDMS composite sample was firstly irradiated with a UV light of 365 nm for 1 min before the test. The intensity of afterglow decreases gradually after UV irradiation. Therefore, for the sample exhibiting relatively strong afterglow emission, the frictional force was applied 5 min after the UV irradiation, while 10 min was waited for the sample exhibiting weak afterglow emission. The two pictures were taken in two separate trials and for both cases, the same shutter duration of 10s was used.

The frictional force was applied by rubbing the CBTZ-Pr /PDMS sample continuously during the photo taking period (~0.3 cm^2). by a glass stick. The tip of this glass stick was blunted to avoid any destructive damage to the sample. Owing to the good transparency of glass, the light emitted beneath the glass stick could be observed. As a result, an obvious difference of intensity can be observed between the region with application of frictional force and the region without frictional force at both time spots (5min and 10min after UV irradiation). Moreover, the difference in intensity of ML between two regions is more obvious when the afterglow remains stronger. The sample shows stronger ML emission when the intensity of afterglow is higher, which would imply the relationship between persistent luminescence (afterglow) and ML.

3.1.2 ML spectrum vs PL spectrum

Figure 3.1.2 shows the spectra of the photoluminescence (PL) and ML emissions of the CBTZ-Pr/PDMS composite sample. Both the spectra show a peak at 611 nm, which is consistent with the observed red ML emission shown in the photographs (Fig. 3.3). The same peak position of PL and ML indicate that the ML emission is resulted from similar electron transitions between different energy levels of the Pr luminescence center; i.e., the $^1D_2 \rightarrow {}^3H_4$ transition of Pr after the effective excitation by UV photons with wavelengths of 250~360nm [41, 53].

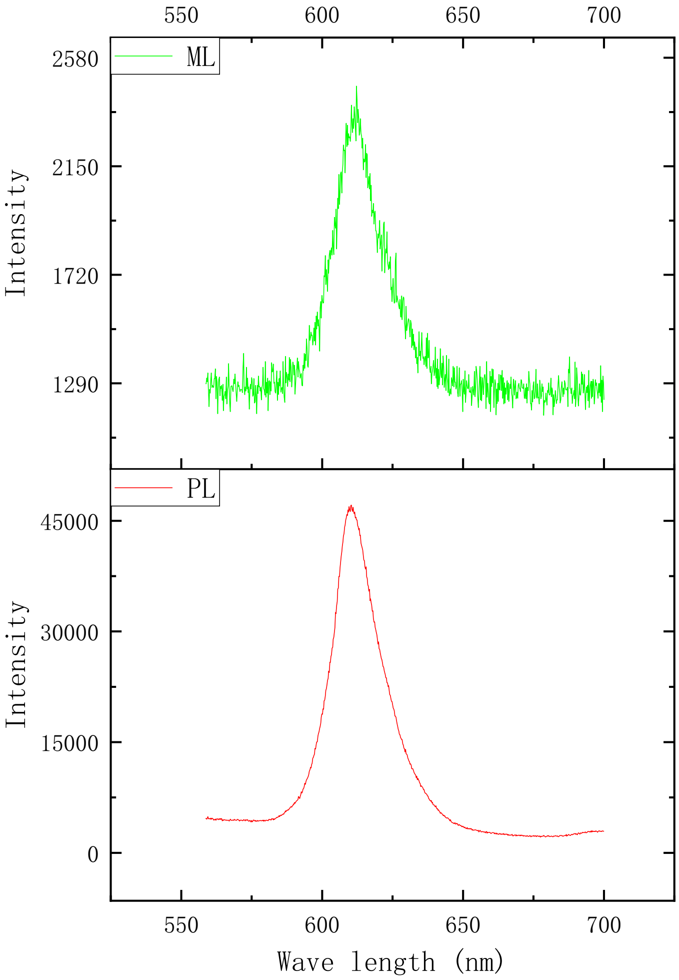

Figure 3.3 ML and PL spectrum of CBTZ-Pr

3.1.3 ML intensity vs Force

The quantitative relationship between the ML intensity and the tensile force is investigated in this section. Before the measurement, the CBTZ-Pr/PDMS composite sample was irradiated with UV light for 1 min. The measurement then started in 10 min to make sure the afterglow emission vanished and provided no effects on the ML measurement. During the measurement, a tensile force of 2 N is applied to the composite sample periodically, i.e., the constant force was applied for 2~4 s and released for ~10s (manually controlled). As shown in Figure 3.4 and 3.5, the ML intensity increases instantaneously when the force is applied and starts to decrease when the force is released. It is noted that the background noise of the PMT is relatively low such that the ML intensity can easily be observed. As also shown in Figure 3.4 and 3.5, the observed ML intensity follows the variation of the tensile force in each cycle, but with the maximum intensity decreasing gradually.

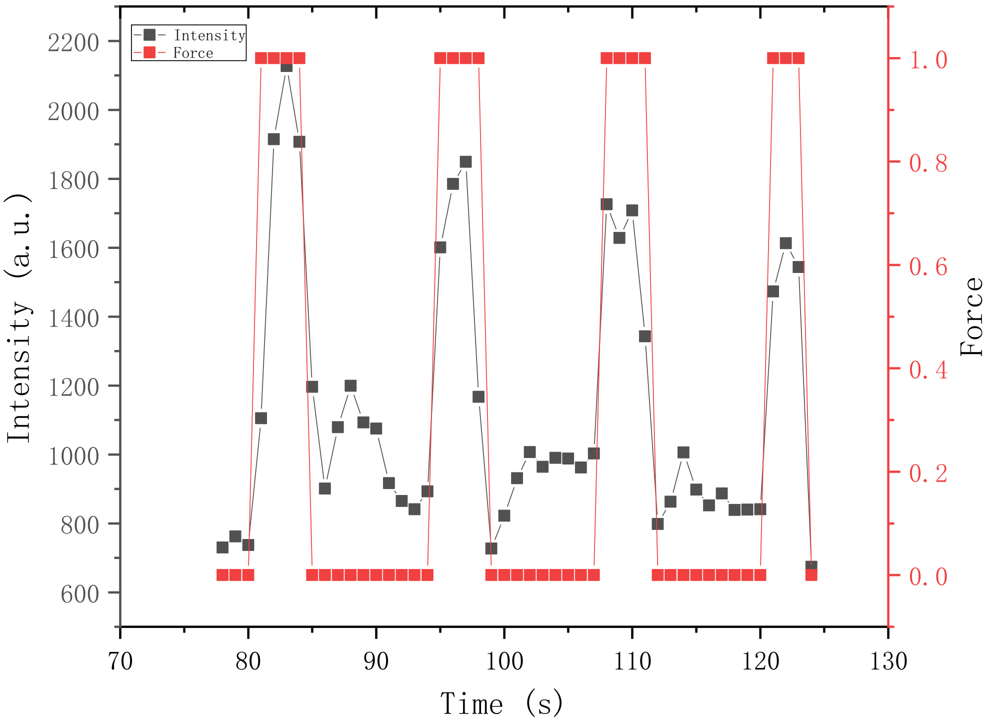

Figure 3.4 Intensity vs time graph after first UV exposure

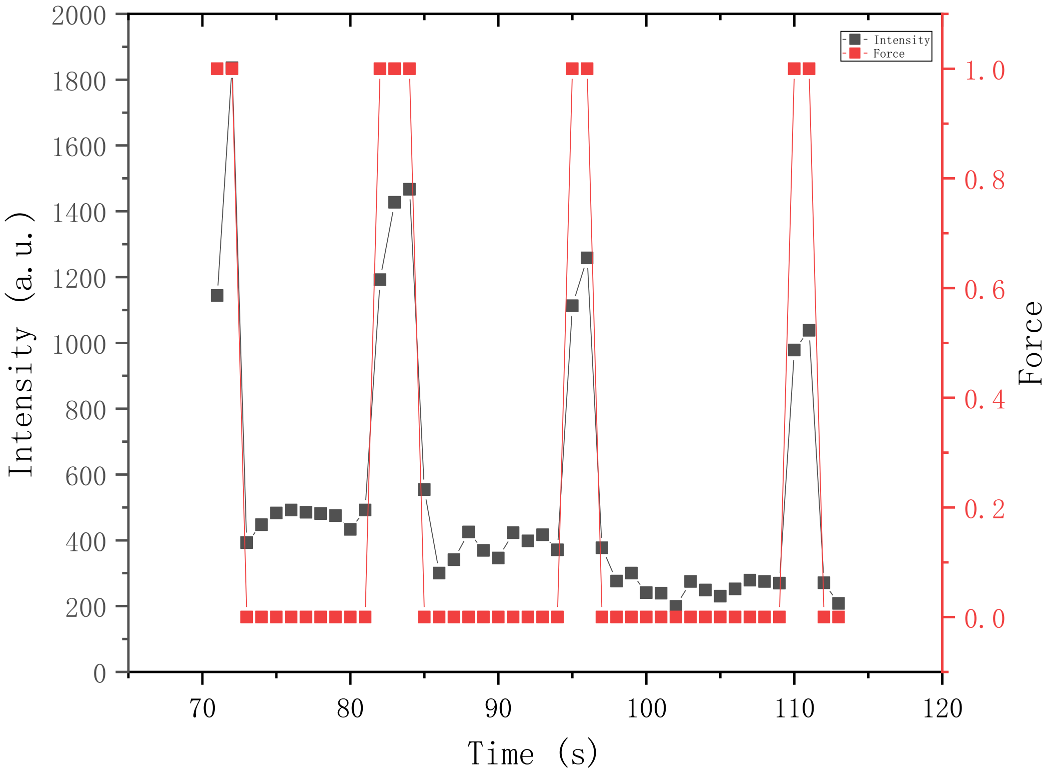

Figure 3.5 Time vs intensity graph after the second UV exposure

To evaluate the restorability of the observed ML response, the composite sample has been re-irradiated with UV light after subject to 4 cycles of tensile force, giving the results shown in Figure 3.5. It is expected that the re-irradiation will “recharge” the trap levels for enhancing the ML response. As shown in Figure 3.5, the observed ML intensity increases after the re-irradiation of UV light, but cannot reach the maximum value in the first cycle of tensile force after the first irradiation of UV light. However, similar to the first irradiation, the observed ML intensity also follows the variation of the tensile force in each cycle, and the maximum intensity decreases gradually in subsequent cycles of tensile force. The variation of the maximum ML intensity with the cycles of tensile force is shown in Figure 3.6:

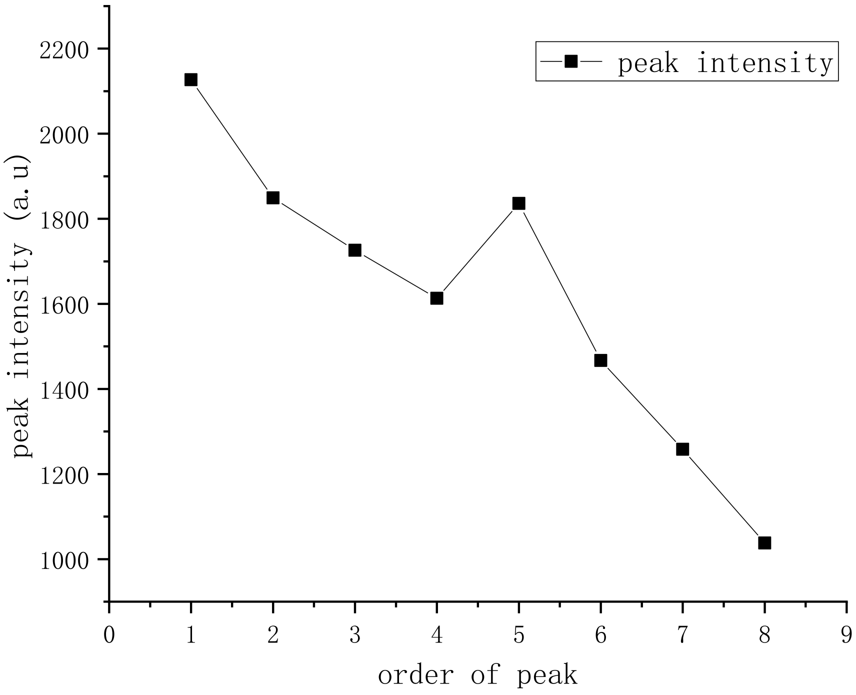

Figure 3.6 Comparation of peak intensity with increase of testing trials

As discussed above, although the ML intensity decreases gradually with the cyclic tensile force, After the recovery by UV light exposure, the intensity would recover partly and also keep decreasing with the testing repeated like the first trial. it can recover partly after the re-radiation with UV light. This suggests that EML (elastico-mechanoluminescence) occurs during the deformation of material. As discussed in Chapter 1, no recovery of ML intensity will be observed when FML or PML occurs. Apart from that, the plastic deformation or fracture of the CBTZ-Pr/PDMS composite sample does not necessarily lead to any permanent deformation of the CBTZ-Pr ceramic inclusion. As the mechanical strength of the ceramic powders is much higher than that of the PDMS matrix, the matrix will obviously deform much more than the inclusion and undergo plastic deformation or even fracture first. Therefore, it is expected that the CBTZ-Pr ceramic powders will only undergo elastic deformation during the whole process.

3.2 Morphology and structure characterization

3.2.1 SEM image of CBTZ-Pr/PDMS sample

Figure 3.7 shows the SEM image of the surface of the CBTZ-Pr/PDMS composite sample. The dimension of the ceramic powders is quite uniform, having an average value of ~20μm. The powders are well combined with PDMS matrix and the distribution is relatively uniform. Although some defects such as small holes are observed, they are smaller than the ceramic powders. It has been noted that the composite sample (with a cross-section area of 1 mm^2) will break at a tensile force of 5 N, which is lower than a pure PDMS sample of the same cross-section area. This may be caused by the ceramic inclusions or the defects.

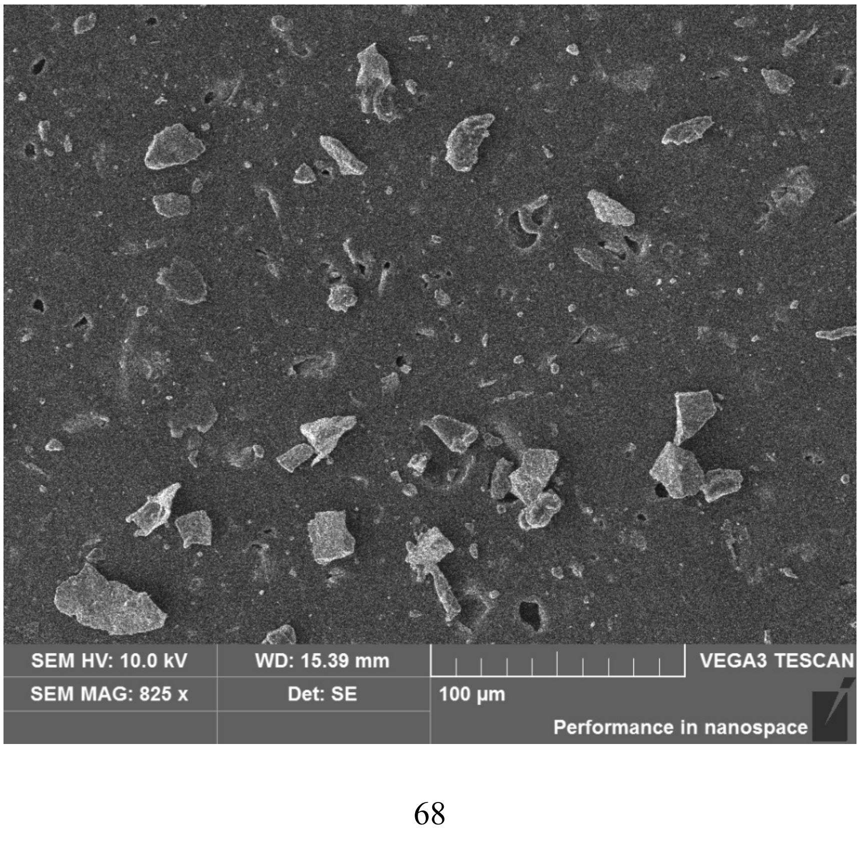

Figure 3.7 SEM image of CBTZ-Pr/PDMS sample

3.2.2 BSE (Back Scattered Electron) image and EDS diagram for diphase crystalline structure analyzation

The BSE images of the CBTZ-Pr ceramic sample are shown in Figure 3.8. Two phases with an obvious difference in brightness can be observed. The intensity of the reflected signal in BSE highly depends on the element composition of the sample. Therefore, the two phases observed in the ceramic should be of different chemical compositions. As shown in the BSE image with lower magnification (Fig. 3.8), the distribution of the two phases is not uniform. Some regions contain one phase (e.g., white phase) more while some regions contain the other phase (e.g., dark phase) more.

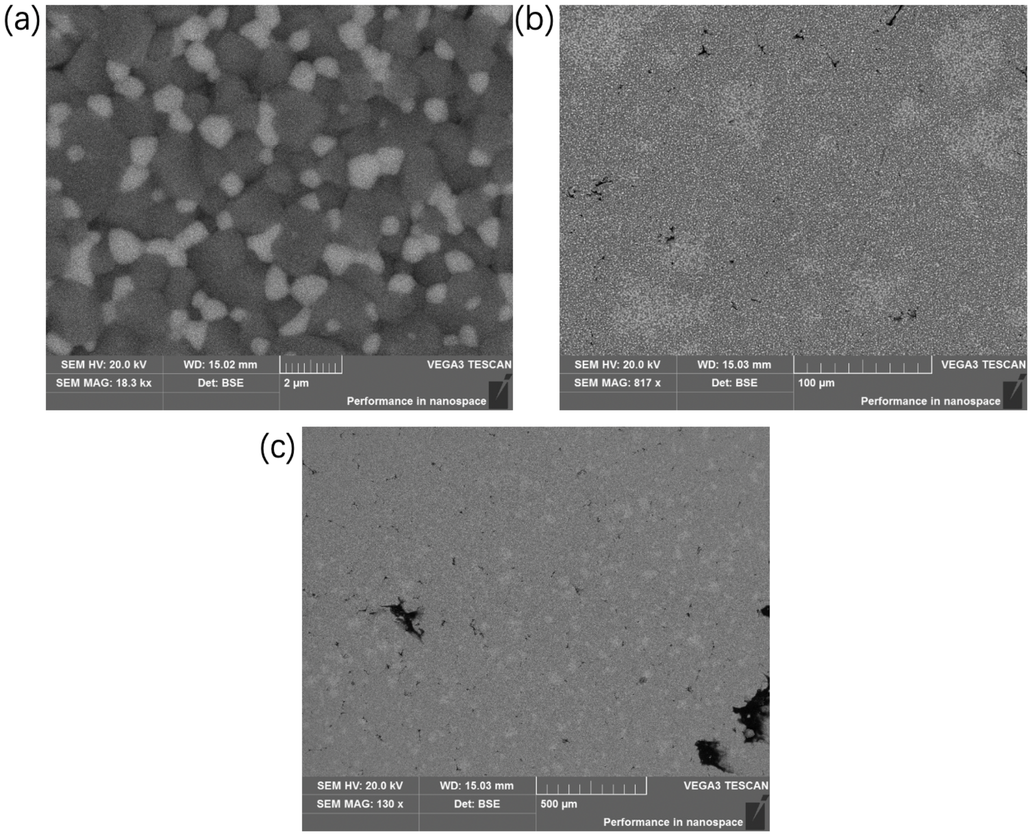

Figure 3.8 BSE image of CBTZ-Pr with magnification value of (a)18300, (b)817, (c)130

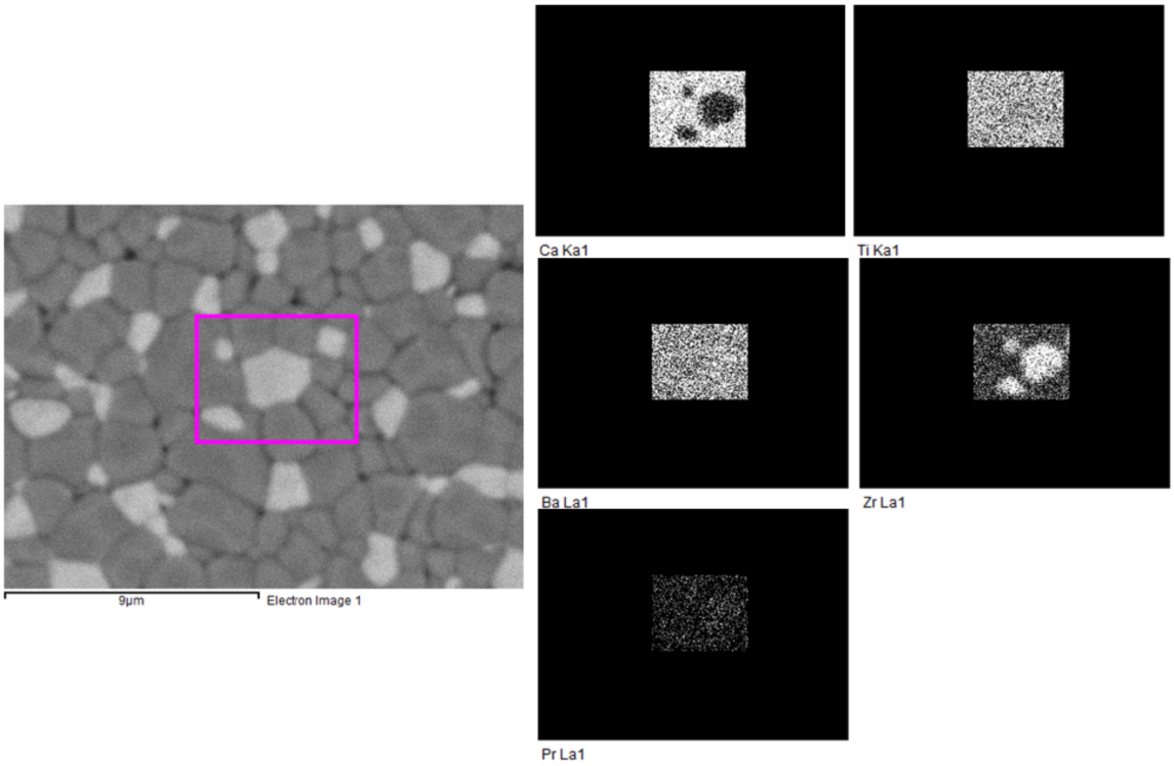

Figure 3.9 Element distribution in white and dark phase

Energy Dispersive X-ray Spectroscopy (EDS) has been conducted on the ceramic sample to investigate the distributions of different elements in the two phases, giving the results shown in Figure 3.8. It can be seen that the distributions of Ba, Ti and Pr are quite uniform across the sample, i.e., the two phases contain similar contents of each of these elements. In contrary, the contents of Ca and Zr in the two phases are different, forming clear boundaries between the phases as shown in the EDS images (Fig. 3.8). As also shown in Figure 3.9, a sharp change in the content is also observed at the boundaries for these two elements, revealing that the white phase contains more Zr and the dark phase contain more Ca. The results also reveal that the white phase contains more Ba and Pr, while the dark phase contains more Ti.

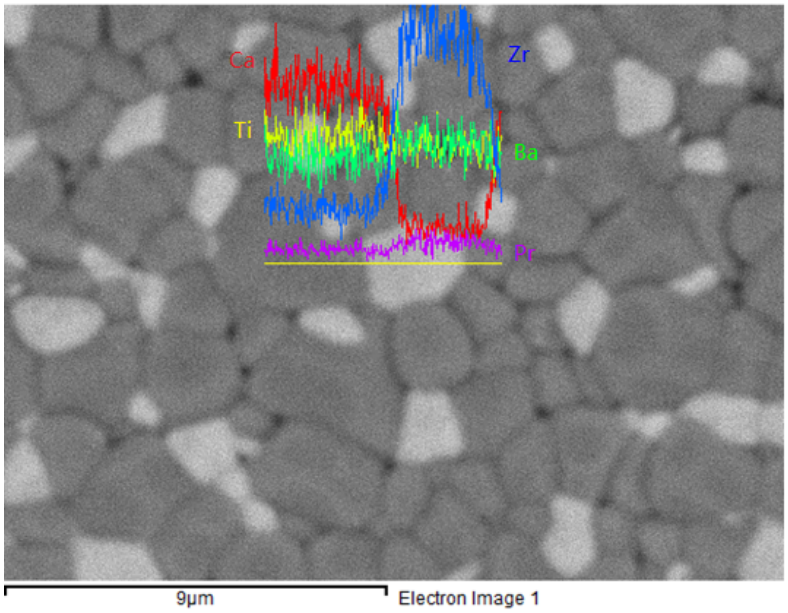

Figure 3.10 Element distribution on the line crossing different phases

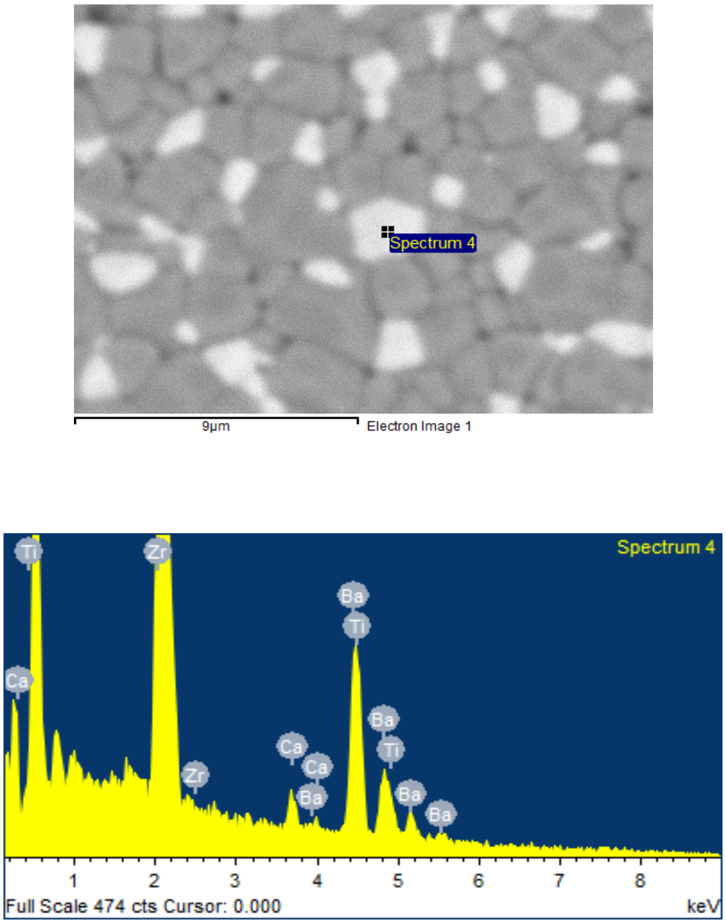

Figure 3.11 EDS spectrum of white phase

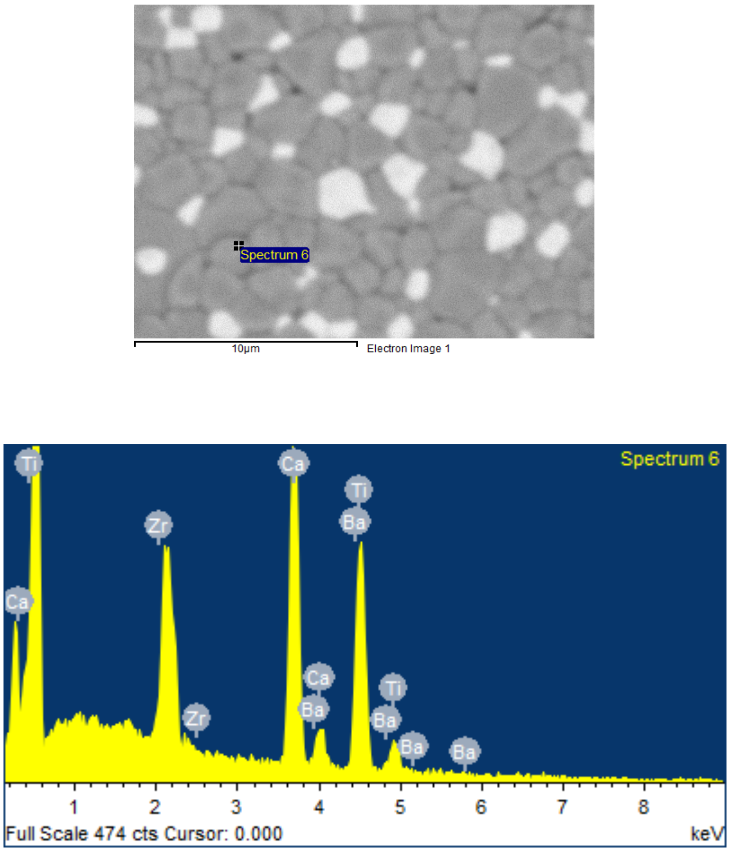

Figure 3.12 EDS spectrum of dark phase

The EDS spectra of the two phases are shown in Figure 3.9. It can be seen that the difference in Ca content between the two phases is much larger than the other elements. Based on the spectra (Fig 3.11, Fig 3.12), the composition of the dark phase is estimated as $Ba_{0.1}Ca_{0.9}TiO_3$: Pr^{3+} and the composition of the white phase is $Ba_{0.93}Ca_{0.07}Ti_{0.2}Zr_{0.8}$:$Pr^{3+}$. The dark phase, $Ba_{0.1}Ca_{0.9}TiO_3$: Pr^{3+} has been explored by many researches while the white phase, $Ba_{0.93}Ca_{0.07}Ti_{0.2}Zr_{0.8}$:$Pr^{3+}$, has not been mentioned in any journal papers.

The record about di-phase structured perovskite can be found in work of Zhang et al[45]. In $Ba_xCa_{1-x}TiO_3$: Pr^{3+}, the composition of single phase changed continuously when x is larger than 0.77 or smaller than 0.1. When the value of x is between 0.1 and 0.77, the ceramic will exhibit di-phase structure with one orthorhombic phase

$Ba_{0.1}Ca_{0.9}TiO_3$ and one tetragonal phase $Ba_{0.77}Ca_{0.23}TiO_3$. The condition of CBTZ-Pr is analogous to this previous work with a similar composition. The crystal structure of Ca-rich phase is similar to $CaTiO_3$ while the structure of Ba-rich phase is similar to $BaTiO_3$. Since the ion radii of Ca and Ba is different, the ratio is naturally controlled in a range to keep the crystal structure stable as orthorhombic and tetragonal. Similarly, the origin of di-phase structure of CBTZ-Pr can also be explain by this reason.

3.3 XRD diagram

Figure 3.13 shows the XRD pattern of CBTZ-Pr powders. By comparison, it is suggested that the ceramic may be composed of two kind of crystal structures: $CaTiO_3$ (COD ID: 1000022) and $BaZrO_3$ (COD ID: 1532743). $CaTiO_3$ has an orthorhombic structure (Pbnm) and $BaZrO_3$ has a cubic structure (Pm-3m). The XRD pattern is well matched to theoretical crystallographic models. Based on these two models, a Rietveld refinement is conducted to determine the crystal structure parameters of CBTZ-Pr.

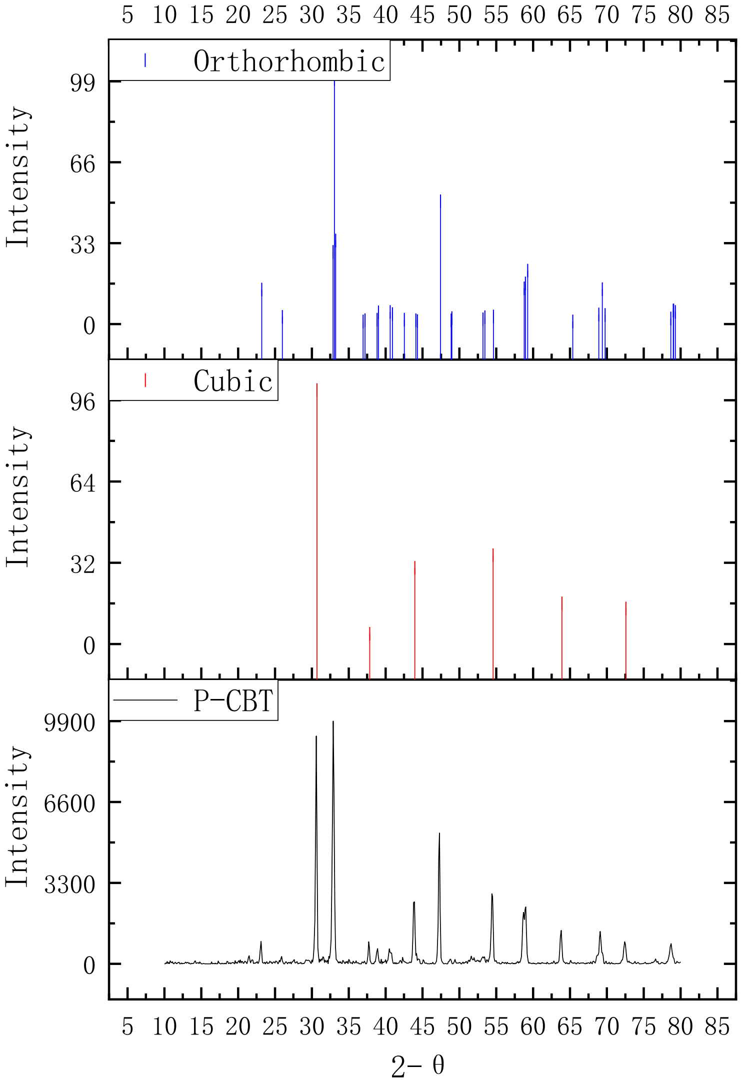

Orthorhombic
Cubic
P-CBT
Intensity
99
66
33
0
96
64
32
9900
6600
3300
5 10 15 20 25 30 35 40 45 50 55 60 65 70 75 80 85
2- θ

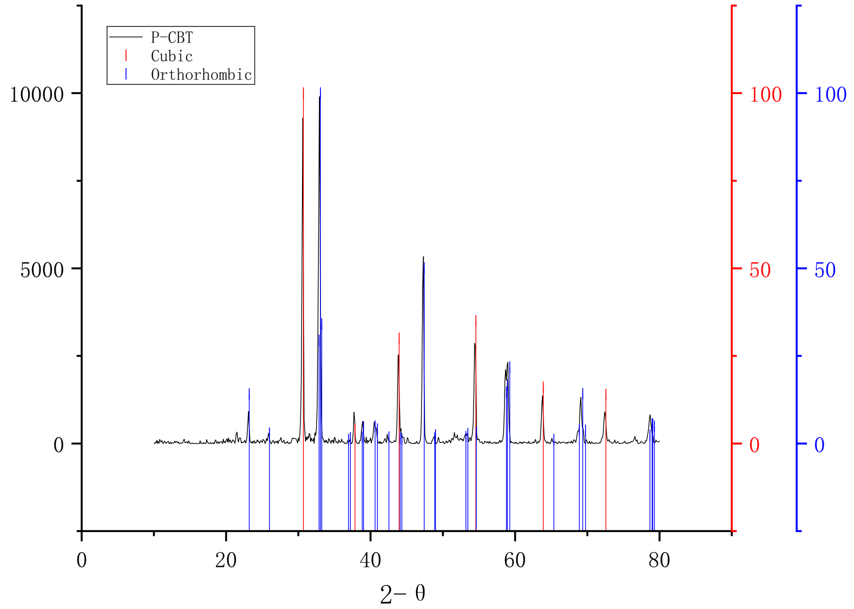

Figure 3.13 Powder XRD pattern of CBTZ-Pr, $CaTiO_3$ and $BaZrO_3$

The Rietveld refinement XRD pattern is shown in Figure 3.14, with each peak classified to the phase it belongs to. By inputting the known parameters (the composition of each phases and the ratio of each element) and adjusting unknown parameters (cell parameters, atom site occupancy and parameters related to strain and texture), the calculated spectra can fit the experiment data well. R_{wp} (weighted profile R-factor), the factor indicating the wellness of the refinement is 9.85%, which is satisfactory and proves the primary assumption of the Bravais lattice and space groups.

The $CaTiO_3$ orthorhombic phase has been shown non-piezoelectric by previous studies[45]. On the other hand, the centrosymmetric $BaZrO_3$ cubic phase does not exhibit piezoelectricity, either. As no polar phases exist, the CBTZ-Pr ceramic is non-ferroelectric.

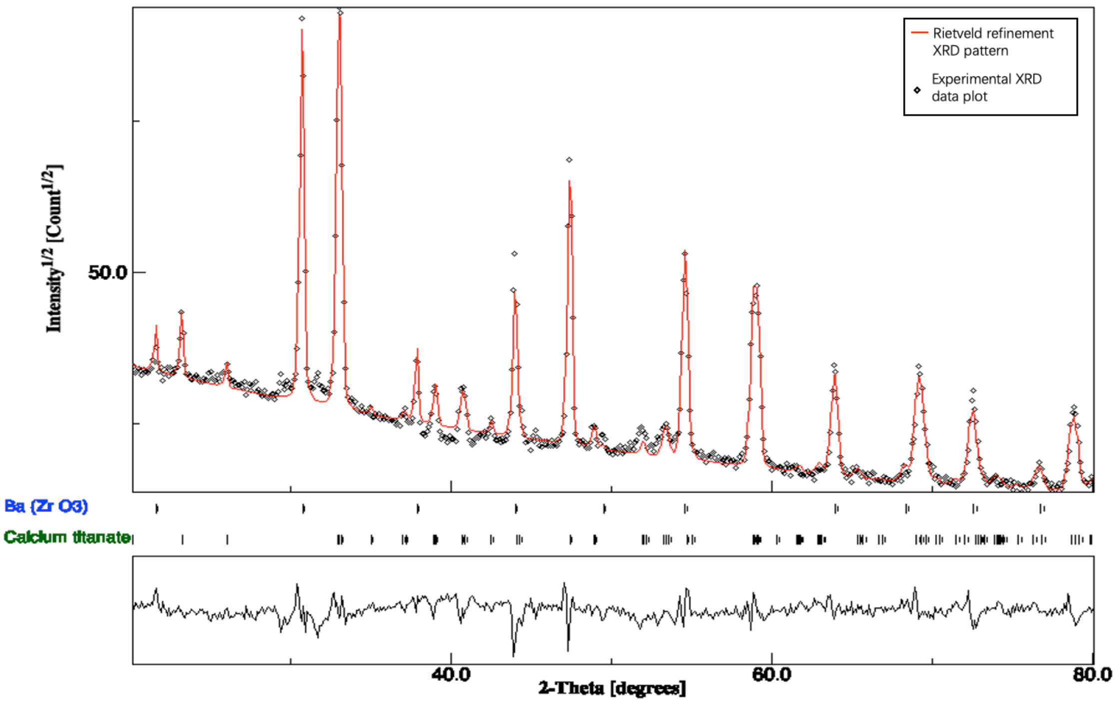

Figure 3.14 Rietveld refinement XRD pattern

3.4 Thermoluminescence glow curve

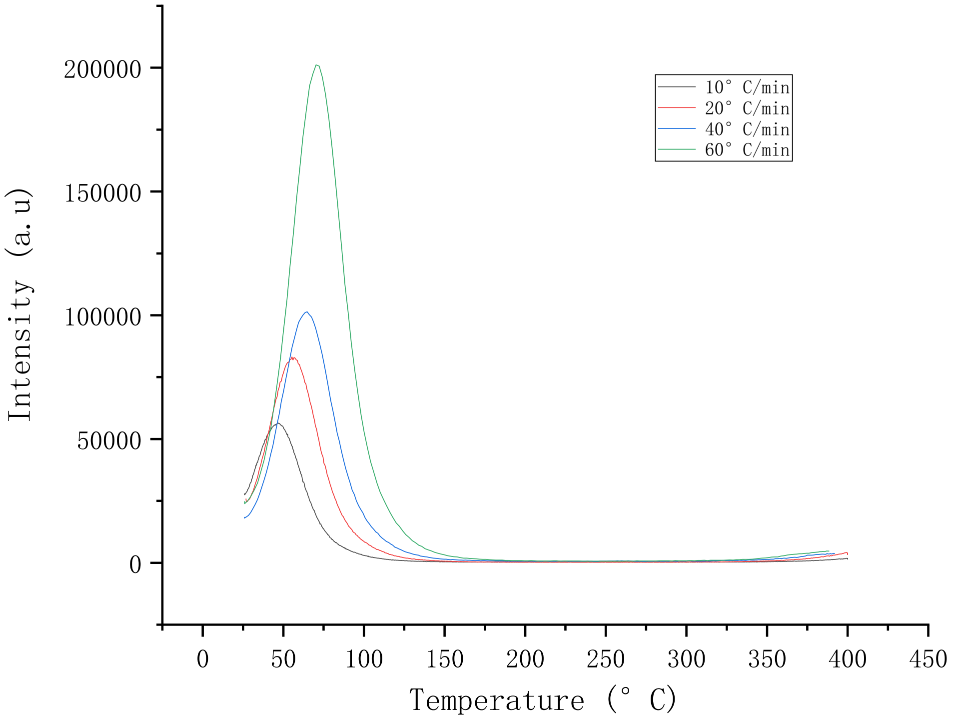

Figure 3.15 Thermoluminescence curve with different heating rate

Figure 3.15 shows the thermoluminescence (TL) glow curves if the CBTZ-Pr ceramic at different heating rates. It can be seen that the intensity peak (both the magnitude and temperature) is highly dependent on the heating rate. The maximum intensity of the peak increases while the peak shifts to higher temperatures with increasing the heating rate.

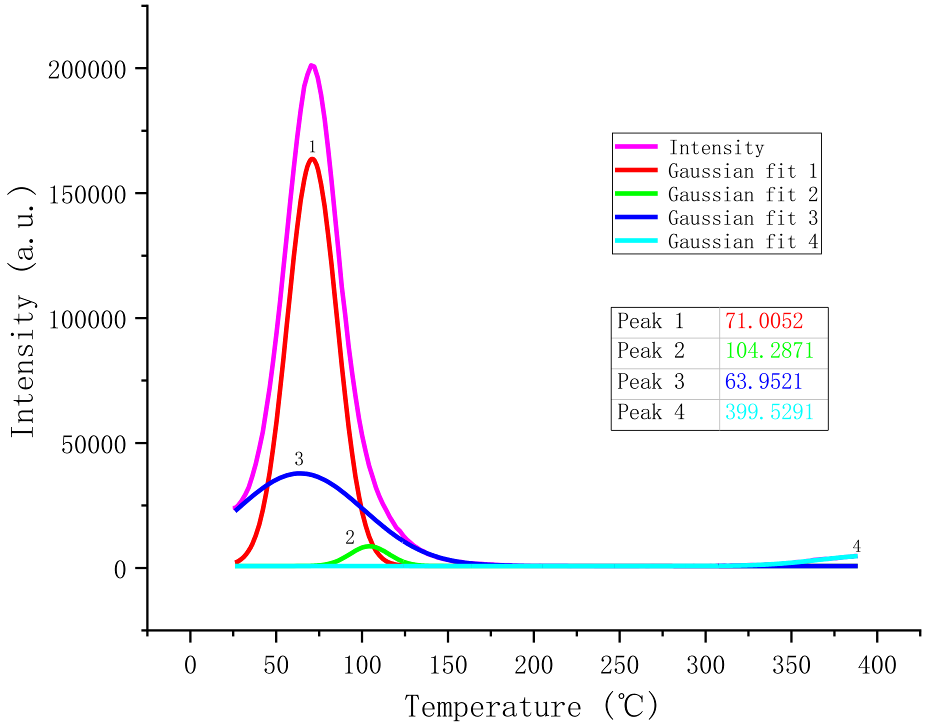

Figure 3.16 Gaussian fitting peaks of TL glow curve with Heating rate=1K/s

The TL glow curve at a heating rate of 60 °C/min (or 1 K/s) has been resolved into different Gaussian-shaped peaks, giving the result shown in Figure 3.16. Peak 1 is considered as the main peak of this TL glow curve, which should be related to the trap levels responsible for the red-light emission.

In order to evaluate the activation energy, the kinetics order has been determined. Following the method discussed in Section 2.2.4, the values of Δ (correction factor) for different Gaussian-shaped peaks are calculated as follows:

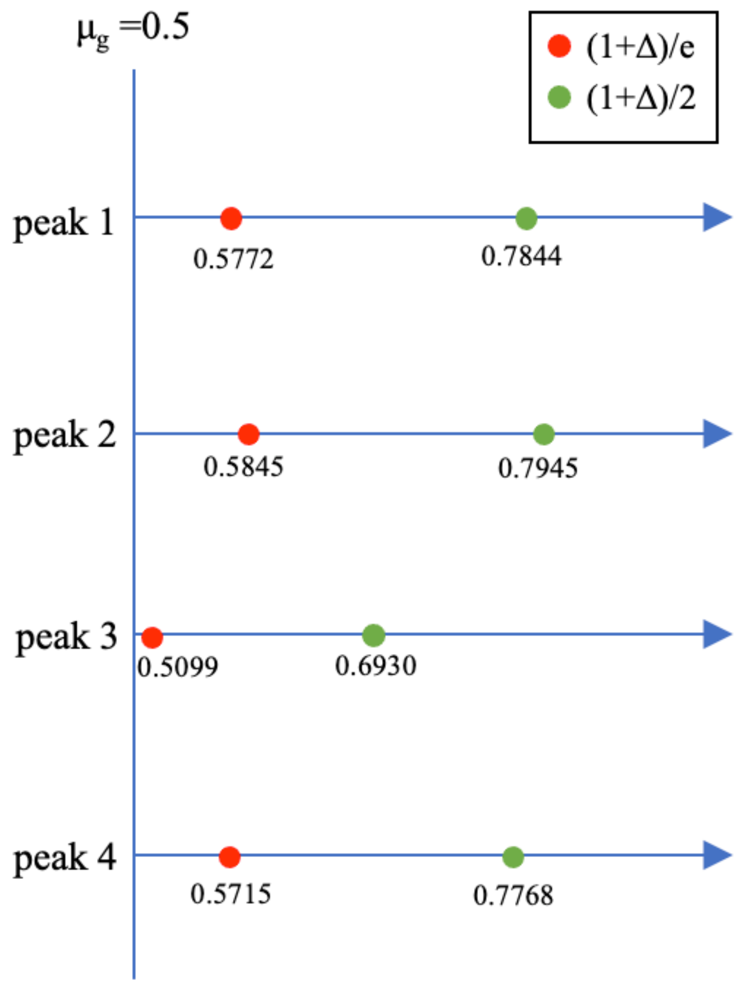

Figure 3.17 Correction factor for determination of kinetics order

As shown in the Figure 3.17, the μ_g value is close to (1+Δ)/e for all of the peaks, suggesting that they all follow the 1st order kinetics in this TL measurement (The value of μ_g is closer to. Accordingly, the activation energy E is estimated suing the equation proposed by Chen et al. as follow[84]:

$$E = 2kT_m(1.26T_m/\omega - 1) \tag{3.1}$$

Where ω is the full width of half-peak magnitude, k is the Boltzmann constant and T_m is the temperature with maximum TL intensity. Similarly, the frequency factor s is estimated as follow:

$$s = [2\beta(\frac{1.26T_m}{\omega} - 1\ )/(e^2 T_m)]exp(2.52T_m/\omega) \qquad (3.2)$$

where β is the linear heating rate in the unit of K/s. The frequency factor s with the unit of s^{-1}indicates the recombination rate of trapped electrons. The calculated activation energy and frequency factor are listed below:

	Peak 1	Peak 2	Peak 3	Peak 4
ω	34.05	26.56	87.28	76.58
T_m in K	344.00	377.29	336.95	672.53
E (in eV)	0.70	1.11	0.23	1.18
S (s^{-1})	$1.05x1^{09}$	$4.24x10^{13}$	52.08	$1.65x10^{7}$

Table 3.1 Activation energy (E) and frequency factor (s) for all the Gaussian-shaped peaks.

With the activation energy, the energy level diagram can be constructed for investigating the ML process. However, the data of peak 4 is not valid since the full peak shape is not presented in the temperature range. The temperature corresponding to peak 4 is also too high for traps participating luminescence. Therefore, the peak 4 should not be considered as effective data for trap analyzation in following part.

In the following chapter, discussion about the experiment data and proposed models of ML will be given. Different models of mechanism will be evaluated based on the experiment results and a possible mechanism will be proposed to elucidate the ML process in CBTZ-Pr.

Chapter 4 Mechanism of Mechanoluminescence

4.1 Mechanism analysis

Although researches have been conducted to develop new mechanoluminescence (ML) materials and enhance the ML emissions, the underlying mechanism of the ML process is still not completely understood. In fact, many efforts have been made to explore the mechanism of ML. However, till nowadays, there are still no general mechanisms that can work on all the ML materials. This is mainly attributed to the complexity of the ML process, with many unknown or known complicated factors existed during a trial of reaction. Firstly, the mechanical load may result in thermal energy produced from the high temperature and high pressure generated at the tip of crack during its propagation. Apart from thermal energy, electrical potential may be also possibly produced in the ML process due to the movement of charged dislocation and the change of charge distribution, which is induced by the difference of electrical potential between the material and the tool applying mechanical load. The environment of the ML materials, especially the surrounding gas is also important since discharge of them will cause light emission and subsequently tribophotoluminescence. Subjected to all these uncertain factors and many other unknown factors, the research progress of the ML mechanism is relatively limited compared to the development or improvement of ML materials. Nevertheless, it is meaningful to discuss the existing mechanisms before exploring the mechanism, based on the experiment results presented in Chapter 3, of EML observed in the CBTZ-Pr/PDMS composite sample.

In an extrinsic ML material, the excitation energy will be absorbed by the host lattice and then be transferred to the luminescent centers, which are always the dopants added to the material. The luminescence in extrinsic ML material can be classified into two types: unlocalized luminescence and localized luminescence. Unlocalized luminescence contains the production and recombination of free charge carriers, which does not have geometrical restrict. For localized luminescence, the excitation and light emission are related to the luminescence centers. Since our ML spectra have shown that the ML observed in the CBTZ-Pr/PDMS composite samples is arisen from the electron transition of the Pr luminescent center, it is considered as localized luminescence in exploring the mechanism of the ML process in the composite sample.

It is commonly accepted that ML is induced by the transitions of charge carriers at trap levels. The release of trapped electrons can excite the luminescent centers, which then relax back to the ground state with the emission of light. There are a number of mechanisms proposed for explaining how the trapped electrons excite the luminescence centers. It has been suggested that a polar crystalline structure is necessary for materials to exhibit ML[89]. However, Chandra et al. [90] have shown that some ML inorganic sulphates having centrosymmetric structure can also exhibit ML. According to literatures[9] , there are only 53% of sulfates, 50% of nitrates, 68% of aromatic organic compounds exhibiting ML are non-centric. These suggest that the origin of ML may not be fully correlated to piezoelectricity[91]. The existing mechanisms can be roughly classified into three types, piezoelectricity induced ML, electric field (produced by domain structures) induced ML and movement of dislocation induced ML.

4.2 Existing ML models

4.2.1 Piezoelectricity induced ML

In materials exhibiting piezoelectricity, an internal electric field will be induced when a mechanical load is applied to it. The electric field can help to release the trapped charge carriers and then trigger the excitation of the luminescent centers. Figure 4.1 shows the energy level diagram for the ML process occurred in ZnS: Mn^{2+}.

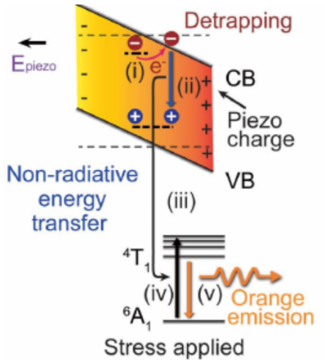

Figure 4.1 Energy band diagram of piezoelectricity induce ML in ZnS: Mn^{2+}[25]

As shown in Figure 4.1, the internal electric field tilts the conduction band and valence band, and thus de-trapping the trapped electrons. The de-trapped electrons have a non-radiative recombination with holes and release energy, which is transferred to the Mn^{2+} luminescence centers, triggering the outer shell electrons to higher energy levels. When the excited ions relax back to the ground state, photons will be emitted as the ML emission.

4.2.2 Electric field (produced by domain structures) induced ML

Apart from piezoelectricity, domain structures can also generate internal electrical fields. Many researchers have shown that domains and domain walls are related to ML [92, 93]. Zhang et al. have studied the ML of $BaTiO_3$-$CaTiO_3$: Pr^{3+}. The sample is a diphase ceramic, containing tetragonal ferroelectric phase $Ba_{0.77}Ca_{0.23}TiO_3$ and another non-piezoelectric orthorhombic phase $Ba_{0.1}Ca_{0.9}TiO_3$[94]. The Ca-rich phases interacts with the Ba-rich phase at the boundary, resulting in a high electrostrictive strain, which amplifies the piezoelectricity-induced electric field when a mechanical load is applied to the material. According to the proposed a sandwich structure model in which the Ca-rich phase is surrounded by the Ba-rich phases (Figure 4.2), an electric potential will be induced across the domains of Ca-rich phase by the piezoelectricity of the Ba-rich phase. As a result, the luminescence centers in the Ca-rich phase will be excited and emit light.

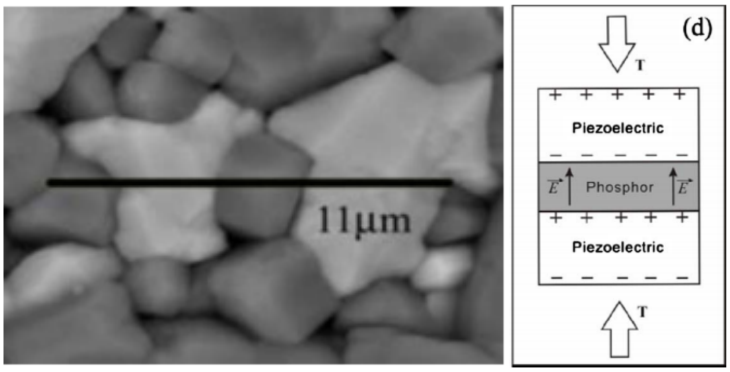

Figure 4.2 Sandwich structure in $BaTiO_3$-$CaTiO_3$: Pr^{3+}[94]

4.2.3 Movement of dislocation induced ML

Not all the proposed mechanisms require and electric field to induce ML emissions. It has been suggested that the ML observed in alkali halides is induced by the movement of dislocation when the force is applied to the materials. The process requires the participation of defects in alkali halides, such as F-centers, V_k-centers and impurity centers. The movement of dislocation will help the recombination of electrons in F-centers and holes in V_k-centers. The schematic diagram is shown in Figure 4.3.

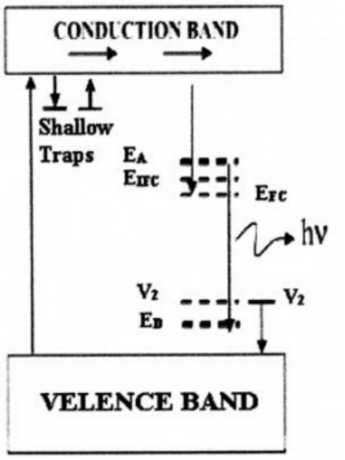

Figure 4.3 Schematic diagram of ML induced by movement of dislocation [95]

As perovskites generally do not contain the above-mentioned defects, the theory is then applicable to them. However, the movement of defects still exist during the deformation of crystal structure. The recombination triggered by the movement is driven by another working principle: tunneling mechanism.

4.2.4 Tunneling mechanism

In order to better understand the origin of tunneling mechanism, it is necessary to have an introduction of the anomalous fading effect. Anomalous fading effect refers to the shorter half-life of persistent luminescence than the theoretical value calculated based on the activation energy (E) and frequency factor (s). The half-life of trapped charge carriers can be calculated by [96]:

$$\tau = s^{-1} exp(E/kT) \tag{4.1}$$

As shown in Chapter 3, the calculated frequency factor s for the main Gaussian-shape peak of the TL glow curve for the CBTZ-Pr ceramic is in order of 10^9. Therefore, the calculated half-life is then in unit of years, which does not agree with the which does not agree with the observations even for the cases the temperature has been well controlled under the peak temperature of TL glow curves [97-100]. It has been suggested that the shorter half-life, named as anomalous fading, is resulted from the loss of trapped charge carriers in a non-thermal way, and a tunneling mechanism has been proposed to explain the process.

If the energy levels of the traps and recombination centers are geometrically adjacent to each other, the wave functions of trapped carriers will be superimposed. As a result, the charge carriers can transit between the traps and recombination centers though the tunneling effect. The recombination center, which is the place where recombination occurs, can be regarded as luminescence center in this case. As shown in the photoluminescence (PL) spectra (Figure 3.3), only one peak can be seen. It indicates that no other recombination emission, i.e., luminescence occurs in the CBTZ-Pr. Therefore, in this thesis, luminescence center is used instead of recombination center in following paragraphs.

Tunneling effect exists in various thermoluminescence materials, and the result is the occurrence of recombination without gaining sufficient energy to delocalize the charge carriers [101, 102]. The tunneling will happen when the trapped charge carriers pass through the potential energy barrier and reach the recombination centers. The possibility of tunneling P can be described in terms of the distance versus distance between the traps and luminescence centers r as [96]:

$$P(r) = P_0 exp\left(-\frac{r}{a}\right) = P_0 exp(-\alpha r) \qquad (4.2)$$

where P_0 and a are constants determined by the compositions of the materials. Apparently, the probability of tunneling increases with decreasing r. When more trapped charge carriers are transferred to the luminescence center by tunneling effect, recombination will occur at the luminescence center, and hence induce luminescence.

4.3 Mechanism of ML in CBTZ-Pr

With various mechanisms have been proposed for ML process, they can be classified into two types: piezoelectric and non-piezoelectric. In fact, the piezoelectricity induced ML model for ZnS: Mn^{2+} is well accepted, since the ML intensity quenches when the piezoelectric coefficient of host lattice is lower. Compared to mechanisms with piezoelectricity involved, the non-piezoelectric mechanisms for EML seldom attract any attentions. This is because the amount of mechanical energy transferred to each atom during elastic deformation (10^{-6}-10^{-5} eV [103]) is much lower than the energy required for direct excitation of luminescence centers (a few eVs) or the releasement of trapped charge carriers (0.7 eV for CBTZ-Pr). It makes a common sense that the mechanical load cannot induce the luminescence directly, so the piezoelectricity has been considered to be the “agent” which help the occurrence of ML emissions.

With this assumption, we fabricate CBTZ-Pr samples trying to combine the strong piezoelectricity of BCTZ-Pr and the strong luminescence of $CaTiO_3$: Pr. However, the fabricated ceramics does not exhibit any piezoelectricity since it naturally turns into two phases, and neither of them is piezoelectric. Although CBTZ-Pr is non-piezoelectric, a strong red-color EML emission still occur in the sample. Therefore, the mechanism for CBTZ-Pr does not contain the involvement of piezoelectricity. At the same time, the mechanical load cannot directly release the trapped charge carriers by transferring the mechanical energy to each atom. Therefore, the tunneling mechanism is the most possible one among the mechanisms proposed by now.

The first evidence is the occurrence of anomalous fading during the persistent luminescence, i.e., afterglow of CBTZ-Pr (the definition of persistent luminescence and afterglow is slightly different, but they can be considered as the same in specific cases). Figure 4.4 presents the afterglow decay curve of CBTZ-Pr. It can be seen that the intensity of afterglow decreases to the level of background noise (around 800 in unit of PMT) after around 300s. It is much less than the calculation result from thermoluminescence curve in Chapter 3. The frequency factor of main peak is in the scale of 10^9, which indicates the theoretical lifetime is several years. The difference between the actual and theoretical lifetime proves the occurrence of anomalous fading effect in CBTZ-Pr, which also indicate the existence of tunneling effect in the ceramics.

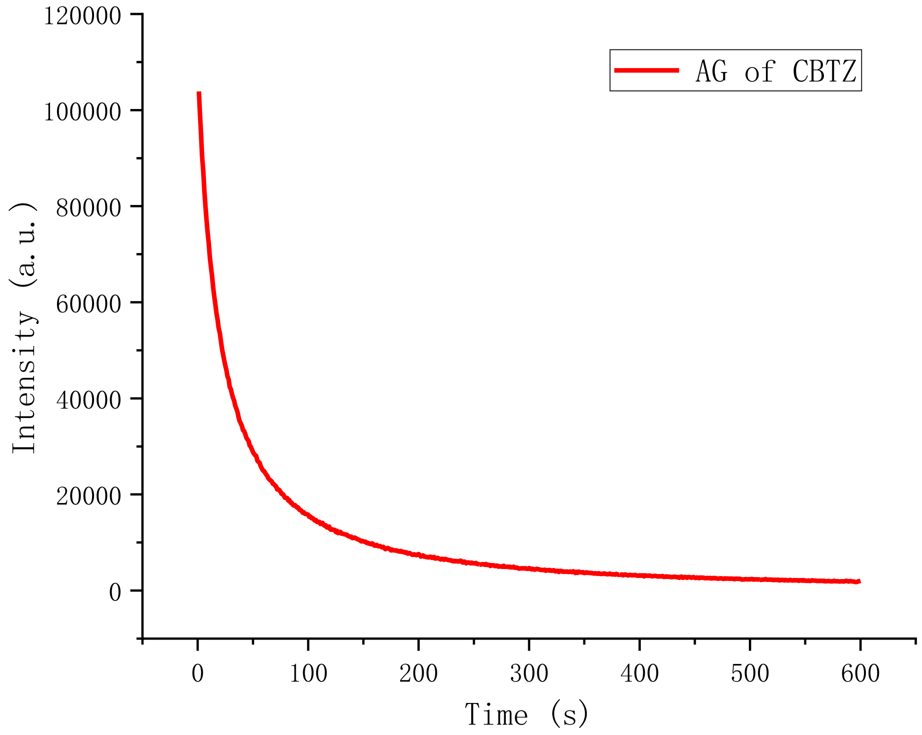

Figure 4.4 Afterglow decay curve of CBTZ-Pr

The second evidence is the dependence of EML intensity on the intensity of afterglow, i.e., the EML emission is stronger when the intensity of afterglow is higher. As shown in Figure 4.5, the EML intensity induced by frictional force in (b) is much stronger than (a). The photos were taken at two trials, so the two EML emissions will not affect each other. It indicates the strong correlation between EML and afterglow.

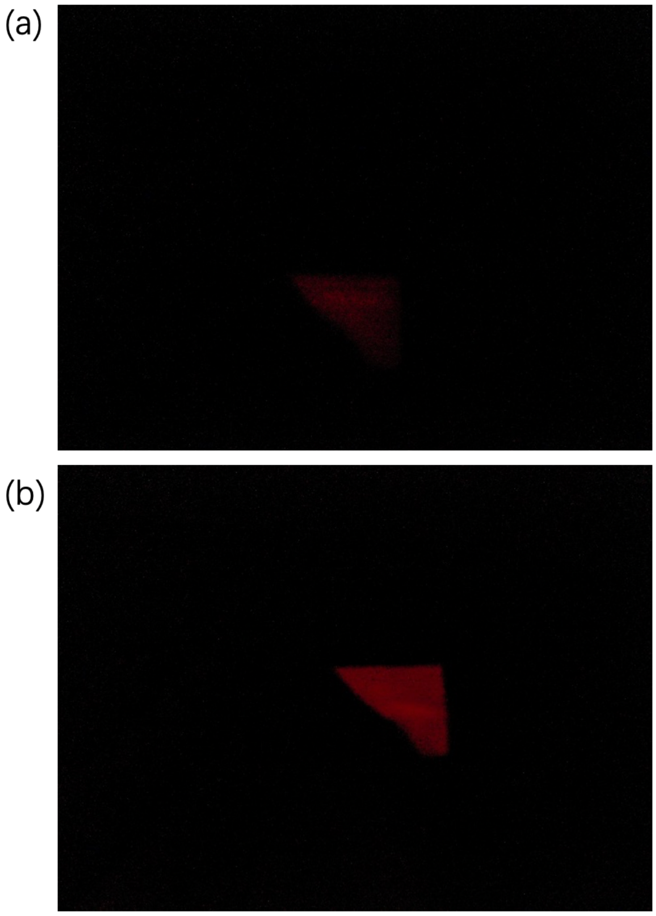

Figure 4.5 Photograph of ML with friction force with afterglow existing (a) weakly and (b) strongly

During the afterglow process, as stated in Clabau persistent luminescence model, electrons will not be released to the conduction band, which is proved by a photoconductivity experiment [104]. Instead, the trapped electrons will be transferred to luminescence center directly, which requires close proximity between the luminescence center and traps. Based on this discovery, Aitasalo proposed that the charge carriers can also transfer between adjacent traps [105]. Charge carriers can move through traps the luminescence centers via tunneling mechanism, since tunneling will happen when the traps are spatially close to each other. When the spatial distance between traps and luminescence center is shortened by external force, the possibility of tunneling will increase and more emissions accordingly occur. The mechanical load "speed up" the afterglow by increasing possibility of tunneling, that is the reason why EML emission is stronger when intensity of afterglow is higher.

As calculated in Chapter 3, 4 kind of traps exist in CBTZ-Pr ceramics. The depth of them is calculated:

	Peak 1	Peak 2	Peak 3
E (in eV)	0.70	1.11	0.23

Table 4.1 Activation energy of traps in CBTZ-Pr

The optimal depth for afterglow is around 0.65 eV [58] and depth of traps for peak 1 is close to this value. Therefore, traps for peak 1 is supposed to be the direct "exit" for electrons to be transferred to luminescence center in both EML emission and afterglow. The activation energy of traps for peak 3 is not suitable for inducement of afterglow, but not as large as the depth of "very deep traps" (around 2 eV [62]). When they are adjacent to traps for peak 1, the trapped electrons for peak 3 can be transferred to traps for peak 1 through tunneling effect. As for traps for peak 2, the depth of them is shallow and will be fully emptied at low temperature. Therefore, they do not participate the EML emission process and afterglow. As a summary, an energy level diagram is constructed for explaining the EML emissions observed in CBTZ-Pr:

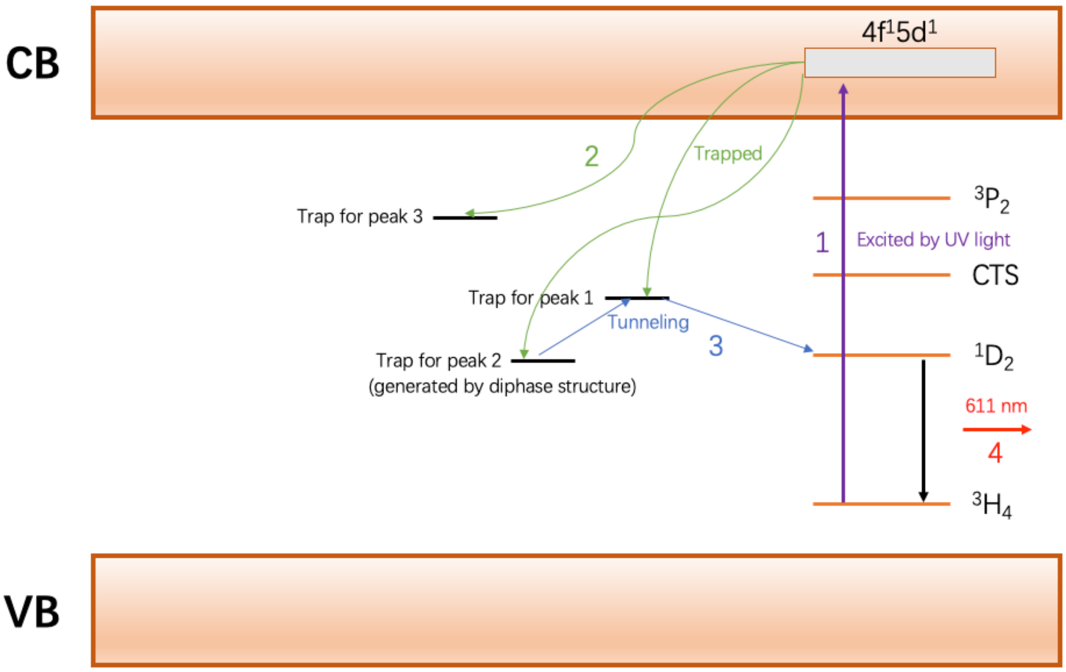

Figure 4.6 Energy level diagram for EML emission

As illustrated in Figure 4.6, 4 steps are required in realizing the EML emissions.

Step 1. Electrons of the Pr^{3+} dopants are excited by UV irradiation to the 4f5d band.

Step 2. Some of the excited electrons relax back to the ground state, while some of them transit to the local traps and become trapped.

Step 3. The external mechanical load generates a strain, which induces a lattice distortion. The distortion decreases the distance between the traps and the luminescence centers, and thus increasing the probability of electron tunneling from the traps to the luminescence centers.

Step 4. Owing to the increased tunneling probability, some of the trapped electrons transit to the adjacent energy levels of Pr^{3+}, and subsequently relax back to the ground state with the emission of photons.

Chapter 5 Conclusion

This study discovers a red-colored elastico-mechanoluminescence (EML) in $Ba_{0.15}Ca_{0.85}Ti_{0.9}Zr_{0.1}O_3$: Pr^{3+} (CBTZ-Pr). Based on the experimental data, a tunneling model is constructed to explain the mechanism of EML emission. The tunneling mechanism does not require the participation of piezoelectricity, which is different from the most of popular ML materials nowadays.

CBTZ-Pr shows a diphase crystalline structure, one is orthorhombic structure, and another is cubic structure. Both phases do not exhibit piezoelectricity. The relationship between EML and afterglow reveals the way of charger carrier transition. Although the energy from mechanical load is not enough for production of free charge carriers, tunneling effect make it possible for charge carriers to transfer though different traps and luminescent centers. However, the tunneling effect requires the proximity of traps and luminescent centers and the transfer is restricted in localized areas, so the intensity of EML emission in CBTZ-Pr is not as strong as piezoelectricity induced ML materials, like ZnS: Mn^{2+}. As non-piezoelectric EML material, the intensity of EML emission in CBTZ-Pr is stronger than expectation, it can provide a new routine for ML materials' development.

The intensity of EML is lowered because of afterglow. As the mechanism stated in the thesis, most charge carriers are released during afterglow. Therefore, by manipulating the depth of traps and decrease the occurrence of afterglow, the intensity of EML can be furtherly increased. In fact, many scientists have proposed this possibility for further improvement of existing ML materials, but there are problems to overcome. For piezoelectric ML materials, the manipulation of trap depth is more difficult, since the trapped charge carriers need to be released into conduction band during the emission. The depth of traps should be shallow enough to be released by piezoelectricity, while deep enough to decrease the occurrence of afterglow. This problem does not exist in tunneling induced ML materials, since the trapped electrons do not need to be excited into conduction band and can transfer to the luminescent centers directly. Therefore, tunneling induced ML materials have a big potential to solve the problem.

Reference List

[1] S-Kei. "PnJunction-LED-E.PNG." Wikipedia. By User:S-kei - File:PnJunction-LED-E.PNG, CC BY-SA 2.5, Link (accessed.

[2] S. Kéna-Cohen, *Strong exciton-photon coupling in organic semiconductor microcavities*. Princeton University, 2010.

[3] D. Vij, *Luminescence of solids*. Springer Science & Business Media, 2012.

[4] G. Shwetha, V. Kanchana, and G. Vaitheeswaran, "CsMgCl3: A promising cross luminescence material," *Journal of Solid State Chemistry,* vol. 227, pp. 110-116, 2015.

[5] M. W. Rowell, "Donor-Acceptor Pair Luminescence."

[6] A. Baldereschi, "Theory of isoelectronic traps," *Journal of Luminescence,* vol. 7, pp. 79-91, 1973.

[7] A. Aten, J. Haanstra, and H. DeVries, "FLOURESCENCE AND PHOTOCONDUCTION IN TELLURIUM-DOPED CADIUM SULPHIDE," *Philips research reports,* vol. 20, no. 4, pp. 395-&, 1965.

[8] D. Thomas, J. Hopfield, and C. Frosch, "Isoelectronic traps due to nitrogen in gallium phosphide," *Physical Review Letters,* vol. 15, no. 22, p. 857, 1965.

[9] V. Chandra, B. Chandra, and P. Jha, "Models for intrinsic and extrinsic elastico and plastico-mechanoluminescence of solids," *Journal of luminescence,* vol. 138, pp. 267-280, 2013.

[10] A. J. Walton, "Triboluminescence," *Advances in Physics,* vol. 26, no. 6, pp. 887-948, 1977.

[11] F. Bacon, *The advancement of learning*. Macmillan & Company, Limited, 1910.

[12] B. Chandra, "Mechanoluminescence," in *Luminescence of solids*: Springer, 1998, pp. 361-389.

[13] J.-C. G. Bünzli and K.-L. Wong, "Lanthanide mechanoluminescence," *Journal of Rare Earths,* vol. 36, no. 1, pp. 1-41, 2018.

[14] C.-N. Xu, T. Watanabe, M. Akiyama, and X.-G. Zheng, "Direct view of stress distribution in solid by mechanoluminescence," *Applied Physics Letters,* vol. 74, no. 17, pp. 2414-2416, 1999.

[15] L. M. Sweeting, M. L. Cashel, and M. M. Rosenblatt, "Triboluminescence spectra of organic crystals are sensitive to conditions of acquisition," *Journal of luminescence,* vol. 52, no. 5-6, pp. 281-291, 1992.

[16] J. I. Zink, "Triboluminescence of uranyl nitrate," *Inorganic Chemistry,* vol. 14, no. 3, pp. 555-558, 1975.

[17] L. Gmelin, "Handbook of Chemistry, trans," *H. Watts (London, 1848–1872),* vol. 1, p. 42, 1852.

[18] B. Brady and G. A. Rowell, "Laboratory investigation of the electrodynamics of rock fracture," *Nature,* vol. 321, no. 6069, pp. 488-492, 1986.

[19] Y. Enomoto, H. Hashimoto, and K. Kikuchi, "Measurements of transient electric current associated with indentation fracture and deformation of brittle solids," *Philosophical Magazine A,* vol. 74, no. 5, pp. 1299-1309, 1996.

[20] N. Aich, A. Appalla, N. B. Saleh, and P. Ziehl, "Triboluminescence for distributed damage assessment in cement-based materials," *Journal of intelligent material systems and structures,* vol. 24, no. 14, pp. 1714-1721, 2013.

[21] G. Alzetta, I. Chudáček, and R. Scarmozzino, "Excitation of triboluminescence by deformation of single crystals," *physica status solidi (a),* vol. 1, no. 4, pp. 775-785, 1970.

[22] C. Xu, T. Watanabe, M. Akiyama, and X. Zheng, "Artificial skin to sense mechanical stress by visible light emission," *Applied Physics Letters,* vol. 74, no. 9, pp. 1236-1238, 1999.

[23] E.-s. IA, "On the Luminescence of γ-rayed KCl crystals induced by plastic deformation," *Journal of the Physical Society of Japan,* vol. 21, no. 11, pp. 2147-2153, 1966.

[24] S. Moon Jeong, S. Song, S.-K. Lee, and B. Choi, "Mechanically driven light-generator with high durability," *Applied Physics Letters,* vol. 102, no. 5, p. 051110, 2013.

[25] X. Wang *et al.*, "Dynamic pressure mapping of personalized handwriting by a flexible sensor matrix based on the mechanoluminescence process," *Advanced Materials,* vol. 27, no. 14, pp. 2324-2331, 2015.

[26] T. Sambrook, C. F. Smura, S. J. Clarke, K. M. Ok, and P. S. Halasyamani, "Structure and physical properties of the polar oxysulfide CaZnOS," *Inorganic chemistry,* vol. 46, no. 7, pp. 2571-2574, 2007.

[27] M. project. "Structure of SrAl2O4 (monoclinic, P2_1, 4)." https://materialsproject.org/materials/mp-3094/ (accessed 2020).

[28] A. Chilvery, S. Das, P. Guggilla, C. Brantley, and A. Sunda-Meya, "A perspective on the recent progress in solution-processed methods for highly efficient perovskite solar cells," *Science and Technology of advanced MaTerialS,* vol. 17, no. 1, pp. 650-658, 2016.

[29] A. K. Jena, A. Kulkarni, and T. Miyasaka, "Halide perovskite photovoltaics: background, status, and future prospects," *Chemical reviews,* vol. 119, no. 5, pp. 3036-3103, 2019.

[30] S. Datta. "Piezoelectric Materials: Crystal Orientation and Poling Direction." https://www.comsol.com/blogs/piezoelectric-materials-crystal-orientation-poling-direction/ (accessed 2020).

[31] V. Goldschmidt, "The laws of crystal chemistry," *Naturwissenschaften,* vol. 14, no. 21, pp. 477-485, 1926.

[32] B. Jaffe, *Piezoelectric ceramics*. Elsevier, 2012.

[33] L. G. Tejuca, J. L. G. Fierro, and J. M. Tascón, "Structure and reactivity of perovskite-type oxides," in *Advances in catalysis*, vol. 36: Elsevier, 1989, pp. 237-328.

[34] M. Pena and J. Fierro, "Chemical structures and performance of perovskite oxides," *Chemical reviews,* vol. 101, no. 7, pp. 1981-2018, 2001.

[35] H. D. Megaw, "Crystal structure of double oxides of the perovskite type," *Proceedings of the Physical Society,* vol. 58, no. 2, p. 133, 1946.

[36] J. Hao, W. Li, J. Zhai, and H. Chen, "Progress in high-strain perovskite piezoelectric ceramics," *Materials Science and Engineering: R: Reports,* vol. 135, pp. 1-57, 2019.

[37] P. F. Smet, B. Viana, S. Tanabe, M. Peng, J. Hölsä, and W. Chen, "Feature issue introduction: persistent and photostimulable phosphors–an established research field with clear challenges ahead," *Optical Materials Express,* vol. 6, no. 4, pp. 1414-1419, 2016.

[38] M. D. McGuinn and S. A. Redfern, "High-temperature ferroelastic strain below the I2/c-I1 transition in Ca1-xSrxAl2Si2O8 feldspars," *European Journal of Mineralogy,* pp. 1159-1172, 1997.

[39] P. Panda, "environmental friendly lead-free piezoelectric materials," *Journal of materials science,* vol. 44, no. 19, pp. 5049-5062, 2009.

[40] G. Lakshminarayana, J. Qiu, M. Brik, G. Kumar, and I. Kityk, "Spectral analysis of RE3+ (RE= Er, Nd, Pr and Ho): GeO2–B2O3–ZnO–LiF glasses," *Journal of Physics: Condensed Matter,* vol. 20, no. 37, p. 375104, 2008.

[41] J. Ganem, W. Dennis, and W. Yen, "One-color sequential pumping of the 4f5d bands in Pr-doped yttrium aluminum garnet," *Journal of luminescence,* vol. 54, no. 2, pp. 79-87, 1992.

[42] W. Jia, D. Jia, T. Rodriguez, D. Evans, R. Meltzer, and W. Yen, "UV excitation and trapping centers in CaTiO3: Pr3+," *Journal of luminescence,* vol. 119, pp. 13-18, 2006.

[43] S. Chadha and A. Vecht, "Electroluminescence," *Springer Proceedings in Physics,* vol. 38, pp. 337-341, 1988.

[44] S. Huang *et al.*, "The spectral properties of the 1S0 state in SrAl12O19: Pr," *Chemical physics letters,* vol. 348, no. 1-2, pp. 11-16, 2001.

[45] J.-C. Zhang, X. Wang, X. Yao, C.-N. Xu, and H. Yamada, "Strong Elastico-mechanoluminescence in diphase (Ba, Ca) TiO3: Pr3+ with self-assembled sandwich architectures," *Journal of the Electrochemical Society,* vol. 157, no. 12, p. G269, 2010.

[46] E. Pinel, P. Boutinaud, and R. Mahiou, "What makes the luminescence of Pr3+ different in CaTiO3 and CaZrO3?," *Journal of Alloys and Compounds,* vol. 380, no. 1-2, pp. 225-229, 2004.

[47] Z. Barandiarán, M. Bettinelli, and L. Seijo, "Color control of Pr3+ luminescence by electron–hole recombination energy transfer in CaTiO3 and CaZrO3," *The Journal of Physical Chemistry Letters,* vol. 8, no. 13, pp. 3095-3100, 2017.

[48] C. Delsart and N. Pelletier-Allard, "Probabilities for radiative and nonradiative decay of Pr3+ ion in LaAlO3," *Journal of Physics C: Solid State Physics,* vol. 6, no. 7, p. 1277, 1973.

[49] A. Kaminskii *et al.*, "Growth, spectral and luminescence study of cubic Bi4Ge3O12: Pr3+ crystals," *physica status solidi (a),* vol. 85, no. 2, pp. 553-567, 1984.

[50] J. Van Vliet and G. Blasse, "Luminescence properties of the Pr3+ ion in La1-xPrxMgAl11O19," *Chemical physics letters,* vol. 143, no. 3, pp. 221-224, 1988.

[51] H. Dornauf and J. Heber, "Fluorescence of Pr3+-ions in La1− xPrxP5O14," *Journal of Luminescence,* vol. 20, no. 3, pp. 271-281, 1979.

[52] C. D. M. Donega, A. Meijerink, and G. Blasse, "Non-radiative relaxation processes of the Pr3+ ion in solids," *Journal of Physics and Chemistry of Solids,* vol. 56, no. 5, pp. 673-685, 1995.

[53] P. Boutinaud, E. Pinel, M. Dubois, A. Vink, and R. Mahiou, "UV-to-red relaxation pathways in CaTiO3: Pr3+," *Journal of luminescence,* vol. 111, no. 1-2, pp. 69-80, 2005.

[54] T. Miura, M. Chini, and R. Bennewitz, "Forces, charges, and light emission during the rupture of adhesive contacts," *Journal of Applied Physics,* vol. 102, no. 10, p. 103509, 2007.

[55] E. N. Harvey, "The luminescence of adhesive tape," *Science,* vol. 89, no. 2316, pp. 460-461, 1939.

[56] W. Hoogenstraaten and H. Klasens, "Some properties of zinc sulfide activated with copper and cobalt," *Journal of the Electrochemical Society,* vol. 100, no. 8, p. 366, 1953.

[57] D. Wang, Q. Yin, Y. Li, and M. Wang, "Concentration quenching of Eu2+ in SrO· Al2O3: Eu2+ phosphor," *Journal of luminescence,* vol. 97, no. 1, pp. 1-6, 2002.

[58] T. Matsuzawa, Y. Aoki, N. Takeuchi, and Y. Murayama, "A new long phosphorescent phosphor with high brightness, SrAl2 O 4: Eu2+, Dy3+," *Journal of the Electrochemical Society,* vol. 143, no. 8, p. 2670, 1996.

[59] V. Abbruscato, "Optical and Electrical Properties of SrAl2 O 4: Eu2+," *Journal of The Electrochemical Society,* vol. 118, no. 6, p. 930, 1971.

[60] T. Aitasalo *et al.*, "Persistent luminescence phenomena in materials doped with rare earth ions," *Journal of Solid State Chemistry,* vol. 171, no. 1-2, pp. 114-122, 2003.

[61] T. Aitasalo, J. Hölsä, H. Jungner, M. Lastusaari, and J. Niittykoski, "Mechanisms of persistent luminescence in Eu2+, RE3+ doped alkaline earth aluminates," *Journal of Luminescence,* vol. 94, pp. 59-63, 2001.

[62] P. Dorenbos, "Mechanism of persistent luminescence in Eu2+ and Dy3+ codoped aluminate and silicate compounds," *Journal of the Electrochemical Society,* vol. 152, no. 7, p. H107, 2005.

[63] P. Dorenbos, "Mechanism of persistent luminescence in Sr2MgSi2O7: Eu2+; Dy3+," *physica status solidi (b),* vol. 242, no. 1, pp. R7-R9, 2005.

[64] T. Wedgwood, "III. Experiments and observations on the production of light from different bodies, by heat and by attrition," *Philosophical Transactions of the Royal Society of London,* no. 82, pp. 28-47, 1792.

[65] F. G. Wick, "An experimental study of the triboluminescence of certain natural crystals and synthetically prepared materials," *JOSA,* vol. 27, no. 8, pp. 275-285, 1937.

[66] A. Ruys, "Processing, structure, and properties of alumina ceramics," *Alumina Ceramics: Biomedical and Clinical Applications, 4th ed.; Woodhead Publishing: Duxford, UK,* pp. 71-121, 2018.

[67] J. C. McDonald and G. M. Whitesides, "Poly (dimethylsiloxane) as a material for fabricating microfluidic devices," *Accounts of chemical research,* vol. 35, no. 7, pp. 491-499, 2002.

[68] I. Johnston, D. McCluskey, C. Tan, and M. Tracey, "Mechanical characterization of bulk Sylgard 184 for microfluidics and microengineering," *Journal of Micromechanics and Microengineering,* vol. 24, no. 3, p. 035017, 2014.

[69] M. J. Buerger, *X-ray Crystallography*. Wiley, 1942.

[70] L. Whittig and W. Allardice, "X-ray diffraction techniques," *Methods of Soil Analysis: Part 1 Physical and Mineralogical Methods,* vol. 5, pp. 331-362, 1986.

[71] J. I. Goldstein, D. E. Newbury, J. R. Michael, N. W. Ritchie, J. H. J. Scott, and D. C. Joy, *Scanning electron microscopy and X-ray microanalysis*. Springer, 2017.

[72] Muso. "Principle of EDX." Own work. https://commons.wikimedia.org/w/index.php?curid=3241031 (accessed 2020).

[73] R. Jenkins and J. L. De Vries, *Practical X-ray spectrometry*. Macmillan International Higher Education, 1970.

[74] A. F. McKinlay, "Thermoluminescence dosimetry," 1981.

[75] M. Oberhofer and A. Scharmann, *Applied thermoluminescence dosimetry*. Adam Hilger Ltd., 1981.

[76] S. W. McKeever, *Thermoluminescence of solids*. Cambridge University Press, 1988.

[77] J. T. Randall and M. H. F. Wilkins, "Phosphorescence and electron traps-I. The study of trap distributions," *Proceedings of the Royal Society of London. Series A. Mathematical and Physical Sciences,* vol. 184, no. 999, pp. 365-389, 1945.

[78] F. Urbach, "Zur lumineszenz der alkalihalogenide: II," *Messungmethoden, Sitzungsberichte Akademie der Wissenshaften in Wien,* vol. 139, p. 363, 1930.

[79] G. Garlick and A. Gibson, "The electron trap mechanism of luminescence in sulphide and silicate phosphors," *Proceedings of the physical society,* vol. 60, no. 6, p. 574, 1948.

[80] C. B. Lushchik, "K TEORII TERMICHESKOGO VYSVECHIVANIYA," *Doklady Akademii Nauk SSSR,* vol. 101, no. 4, pp. 641-644, 1955.

[81] A. Halperin and A. Braner, "Evaluation of thermal activation energies from glow curves," *Physical Review,* vol. 117, no. 2, p. 408, 1960.

[82] L. I. Grossweiner, "A note on the analysis of first-order glow curves," *Journal of Applied Physics,* vol. 24, no. 10, pp. 1306-1307, 1953.

[83] P. Keating, "Thermally stimulated emission and conductivity peaks in the case of temperature dependent trapping cross sections," *Proceedings of the Physical Society,* vol. 78, no. 6, p. 1408, 1961.

[84] R. Chen, "On the calculation of activation energies and frequency factors from glow curves," *Journal of Applied Physics,* vol. 40, no. 2, pp. 570-585, 1969.

[85] A. Wrzesinska, "Impurity-Activated Crystalline Phosphors. Their Production and Thermoluminescence Curves," *Acta Physica Polonica,* vol. 2, p. 130, 1958.

[86] D. Curie, "Luminescence in crystals," 1963.

[87] A. Halperin and R. Chen, "Thermoluminescence of semiconducting diamonds," *Physical Review,* vol. 148, no. 2, p. 839, 1966.

[88] A. Halperin, V. Bar, R. Chen, and J. Levinson, "OPTICAL AND ELECTRICAL PROPERTIES OF DIAMOND (OPTICAL AND ELECTRICAL PROPERTIES OF NON METALS)," ISRAEL ATOMIC ENERGY COMMISSION YAVNE SOREQ NUCLEAR RESEARCH CENTRE, 1967.

[89] J. I. Zink, "Squeezing light out of crystals: triboluminescence," *Naturwissenschaften,* vol. 68, no. 10, pp. 507-512, 1981.

[90] B. Chandra and J. I. Zink, "Triboluminescence of inorganic sulfates," *Inorganic Chemistry,* vol. 19, no. 10, pp. 3098-3102, 1980.

[91] B. Chandra, "Squeezing light out of crystals: triboluminescence," *Nuclear Tracks and Radiation Measurements (1982),* vol. 10, no. 1-2, pp. 225-241, 1985.

[92] X. Wang, C. N. Xu, H. Yamada, K. Nishikubo, and X. G. Zheng, "Electro-mechano-optical conversions in Pr3+-doped BaTiO3–CaTiO3 ceramics," *Advanced Materials,* vol. 17, no. 10, pp. 1254-1258, 2005.

[93] H. Matsuo, K. Ikeda, S. Hata, H. Nakashima, H. Yamada, and C. Xu, "Phase transformation behavior and pseudoelastic deformation in SrAl2O4," *Journal of Alloys and Compounds,* vol. 577, pp. S507-S516, 2013.

[94] J.-C. Zhang, C.-N. Xu, S. Kamimura, Y. Terasawa, H. Yamada, and X. Wang, "An intense elastico-mechanoluminescence material CaZnOS: Mn 2+ for sensing and imaging multiple mechanical stresses," *Optics express,* vol. 21, no. 11, pp. 12976-12986, 2013.

[95] B. Chandra, A. Bagri, and V. Chandra, "Mechanoluminescence response to the plastic flow of coloured alkali halide crystals," *Journal of luminescence,* vol. 130, no. 2, pp. 309-314, 2010.

[96] R. Chen and S. W. McKeever, *Theory of thermoluminescence and related phenomena*. World Scientific, 1997.

[97] R. Chen and A. Hag-Yahya, "A new possible interpretation of the anomalous fading in thermoluminescent materials as normal fading in disguise," *Radiation measurements,* vol. 27, no. 2, pp. 205-210, 1997.

[98] C. Bull and G. Garlick, "The luminescence of diamonds," *Proceedings of the Physical Society. Section A,* vol. 63, no. 11, p. 1283, 1950.

[99] W. Hoogenstraaten, "Electron traps in zinc sulphide phosphors," *Philips Research Report,* vol. 13, pp. 515-693, 1958.

[100] A. Wintle, "Detailed study of a thermoluminescent mineral exhibiting anomalous fading," *Journal of Luminescence,* vol. 15, no. 4, pp. 385-393, 1977.

[101] F. Kieffer, C. Meyer, and J. Rigaut, "Is isothermal deferred luminescence in organic glasses due to electron tunnelling?," *Chemical Physics Letters,* vol. 11, no. 3, pp. 359-361, 1971.

[102] I. Bailiff, S. Bowman, S. Mobbs, and M. Aitken, "The phototransfer technique and its use in thermoluminescence dating," *Journal of Electrostatics,* vol. 3, no. 1-3, pp. 269-280, 1977.

[103] M. Carpenter, C. Howard, M. Andrew, R. McKnight, Y. Liu, and R. Withers, "Elastic anomalies due to structural phase transitions in mechanoluminescent Sr Al 2 O 4: Eu," *Journal of Applied Physics,* vol. 107, no. 1, p. 013505, 2010.

[104] F. Clabau *et al.*, "Mechanism of phosphorescence appropriate for the long-lasting phosphors Eu2+-doped SrAl2O4 with codopants Dy3+ and B3+," *Chemistry of Materials,* vol. 17, no. 15, pp. 3904-3912, 2005.

[105] T. Aitasalo, J. Hölsä, H. Jungner, M. Lastusaari, and J. Niittykoski, "Thermoluminescence study of persistent luminescence materials: Eu2+-and R3+-doped calcium aluminates, CaAl2O4: Eu2+, R3+," *The Journal of Physical Chemistry B,* vol. 110, no. 10, pp. 4589-4598, 2006.